Immunoinformatics design of a novel multiepitope vaccine candidate against non-typhoidal salmonellosis caused by *Salmonella* Kentucky using outer membrane proteins A, C and F

Elayoni E. Igomu[1*¶], Paul H. Mamman[2¶], Jibril Adamu[2], Maryam Muhammad[3&], Abubarkar O. Woziri[2&], Manasa Y. Sugun[1&], John A. Benshak[4&], Kingsley C. Anyika[3&], Rhoda Sam-Gyang[1&] and David O. Ehizibolo[5¶]

[1] Bacterial Vaccine Production Department, National Veterinary Research Institute Vom, Plateau State, Nigeria

[2] Department of Veterinary Microbiology, Ahmadu Bello University Zaria, Kaduna State, Nigeria.

[3] Bacterial Research Department, National Veterinary Research Institute Vom, Plateau State, Nigeria

[4] Biotechnology Center, National Veterinary Research Institute Vom, Plateau State, Nigeria

[5] Foot and Mouth Disease Department, National Veterinary Research Institute Vom, Plateau State, Nigeria

* Corresponding author

Email: elayonigomu@gmail.com (EEI)

¶ These authors contributed equally to this work

& These authors also contributed equally to this work

Abstract

Salmonella Kentucky is a public health threat and responsible for the spread of antimicrobial resistance determinants in human and livestock population across the globe. It is ubiquitous in Africa and an emerging cause of human non-typhoidal gastroenteritis on the continent. In this study, bioinformatics tool was used to design an epitope peptide-based vaccine using outer membrane proteins A, C and F of *Salmonella* Kentucky. We predicted 14 CD8+ and 7 CD4+ T-cell epitopes, putatively restricted by MHC class I and class II alleles. The predicted T-cell epitopes will provide a 94.91 % population coverage when used in a vaccine preparation. Seven highly immunogenic linear B-cell epitopes and 3 conformational B-cell epitopes were predicted. The T-cell and B-cell epitopes were fused using proper linkers to construct a multi-epitope vaccine (MEV). *fliC* protein of *Salmonella* Typhimurium was added at the N-terminal as adjuvant to improve immunogenicity of the peptide construct. The MEV construct had a high quality structure with acceptable physicochemical features. Docking of the MEV against Toll like receptors 1, 2, 4 and 5 and the molecular dynamic simulation of the docked complexes indicated that the formation of these complexes were energetically feasible, stable and strong during immunological activities. Immune stimulation results indicated adequate elicitation of IgG, IgM, CD8+ T-cell, CD4+ T-cell and an array of cytokines (IFN-γ, TGF-b, IL-2, IL-10 and IL-12) with a noticeable decrease in antigen levels. Although the vaccine qualities were commendable, preclinical and clinical trials are required for validation of the protective traits and safety of the designed vaccine.

1. Introduction

Antibiotics are essential tools in modern medicine, indispensable for the treatment of infectious diseases, essential as support therapy in medical interventions (e.g., surgery and cancer

48 chemotherapy), and in livestock and food animal production [1]. The extensive and inappropriate
49 use of antibiotics has fuelled the spread of antibiotic resistance mechanisms in pathogenic bacteria,
50 leading to the very real prospect of a post-antibiotic era. Predictions estimate that by 2050
51 antibiotic resistant bacteria would have killed more people than cancer will [1]. The World Health
52 Organization (WHO) has put across that fluoroquinolone-resistant *Salmonella enterica,*
53 carbapenem-resistant and extended-spectrum *β*-lactamase producing *Enterobacteriaceae* are
54 amongst the highest priority pathogens posing a severe risk to human health [2]. All of these high
55 level resistances have been detected in *Salmonella enterica* subsp. *enterica* serovar Kentucky (*S.*
56 Kentucky). This serovar is considered to be a high risk global Multidrug resistant (MDR) pathogen
57 with well documented zoonotic potential. It has been isolated across different classes of animals
58 and in human [3, 4]. The emergence and continual spread of MDR *S.* Kentucky has been
59 highlighted by different health organizations and nations and its continuous association with high
60 level fluoroquinolone resistance has gained epidemiological importance globally [5].
61 Ciprofloxacin and extended-spectrum cephalosporins are the drug of choice for treatment of severe
62 nontyphoidal *Salmonella enterica* infections in adults. The resistance exhibited by *S.* Kentucky to
63 these choice drugs has left very limited treatment options [3].

64 Vaccines have had an unprecedented impact on human and global health, and have been used for
65 decades, with a much lower probability of resistance emergence when compared with antibiotics
66 [6, 7], as mechanisms of action of vaccines and antibiotics as regards the tendency to generate
67 microbial resistance are intrinsically different and this may account for the lower probability of
68 antimicrobial resistance emergence for vaccines [8]. More so, vaccines are used prophylactically
69 and thus take effect by acting before the bacteria multiplies following initial infection (resulting in

70 a low pathogen burden) and before different tissues and organs are affected, which substantially
71 reduces the likelihood that resistance conferring mutations will emerge and spread [8].
72 *Salmonella* outer membrane proteins (OMPs) have been investigated as potential vaccine
73 candidates over the past several years. The *Salmonella* OMPs viz outer membrane protein A
74 (OmpA), outer membrane protein C (OmpC) and outer membrane protein F (OmpF), are widely
75 distributed and conserved among different *Salmonella* serovars which raises the possibility that
76 they could be used in diagnostics or as part of a subunit or conjugate vaccine [9, 10]. Various
77 studies have shown that a crude preparation of *Salmonella* OMPs evokes strong immune response
78 and induces a protective immunity against infection caused by diverse Gram-negative bacteria
79 [10]. Furthermore, OMPs have surface-exposed epitopes, which are accessible for antibody or T
80 cell receptor recognition [11, 12]. The WHO has highlighted the importance of developing new
81 vaccines against infectious bacterial agents in Sub-Saharan Africa [13, 14] and further expressed
82 that vaccines for nontyphoidal *Salmonella* are urgently required, especially on the continent, as
83 some risk factors makes Africa a critical region in regard to the emergence of antimicrobial
84 resistance [3, 15, 16, 17]. The aim of this study is to design a multi-epitope vaccine (MEV) against
85 Non-typhoidal Salmonellosis (NTS) infection caused by *Salmonella* Kentucky using
86 immunoinformatics and computational methods, from sequences of OmpA, OmpC and OmpF.

87 2. Materials and methods

88 2.1. Retrieval of outer membrane proteins (Omps) of *Salmonella* 89 Kentucky sequences

90 The National Center for Biotechnology Information (NCBI) database was chosen for the
91 retrieval of OmpA, OmpC and OmpF sequences of *S*. Kentucky strains. All the accession number

of OMPs of *S*. Kentucky used were noted (https://www.ncbi.nlm.nih.gov/protein/). To maximize the similarity between proteins of the different strains of *S*. Kentucky OMPs, sequences were blasted with query set at 99 % to 100 % identity (BLAST: https://blast.ncbi.nlm.nih.gov). A sequence of flagellin protein (*fliC*) (GenBank accession number KAA0422324.1) of *Salmonella enterica subsp. enterica* serovar Typhimurium was chosen as an adjuvant to enhance the efficacy of the vaccine peptide [18, 19].

2.2. Multiple sequence alignment of Omps and generation of consensus sequence

The numerous OMPs FASTA sequences were aligned using Jalview (2.11.2.7). Jalview is a free cross-platform program for multiple sequence alignment editing, visualization and analysis (https://www.jalview.org/ [20]. The FASTA sequences of all selected Omp A, C and F from the NCBI database were manually entered on Jalview software program which automatically aligns and generates a predicted consensus sequences using Blosum62 parameters [21].

2.3. Epitope mapping

For the prediction of Cytotoxic T lymphocytes (CTL) and helper T lymphocytes (HTL) activating epitopes, the Immune Epitope Database (IEDB) server (http://tools.iedb.org/main/tcell) was used to predict peptides that bind to major histocompatibility complex class I (MHC-I) and major histocompatibility complex class II (MHC-II), respectively. T-cell epitopes are provided by MHC-I and MHC-II molecules that are recognized by two distinct subsets of T-cells; CD8+ and CD4+ T-cells, respectively [22, 23].

2.3.1. MHC-I epitopes prediction

113 The majority of cytotoxic T-cells have T-cell receptors (TCRs) that identify a particular
114 antigen. Therefore, CTL epitope prediction is critical for vaccine designing concepts. CTL
115 epitopes was predicted on the IEDB recommended 2023.09 (NetMHCpan4.1 EL) server
116 (http://tools.iedb.org/mhci/). The HLA allele reference set was predicted and 9-mer length epitope
117 selected. The threshold for epitope identification for a strong binder was set at 0.5% while at 2%
118 for a weak binder. Peptide binding to MHC-I, proteasomal C-terminus cleavage score, and the
119 transport efficiency of Transporter Associated with Antigen Processing (TAP) was used to make
120 these predictions [23, 24]. The peptide binding to MHC-I and Proteasomal C-terminal cleavage
121 scores was generated using an artificial neural network, whereas the TAP score was calculated by
122 the weight matrix [23, 24].

123 2.3.2. MHC-II epitopes prediction

124 Helper T lymphocytes are a type of adaptive immune cell that may produce humoral and
125 cellular immune responses in reaction to foreign antigens. Hence, HTL epitopes that may bind to
126 MHC-II alleles are critical in vaccine development. HTL epitopes prediction will be performed on
127 online server IEDB (Immune Epitope Database) (http://www.iedb.org/). The 7-allele human
128 leukocyte antigen (HLA) was used as a reference set to predict the epitopes, and HLA-DR was
129 selected for *Homo sapien*. Afterwards, a 15-mer length epitope with a percentile rank classification
130 was obtained (IEDB recommended 2023.05 (NetMHCIIpan 4.1L). The server assigns IC50 values
131 to the predicted epitopes, which are inversely related to the binding affinity towards the MHC-II.
132 IC50 scores of < 50 nM represent a high binding affinity. The IC50 value < 500 nM corresponds
133 to intermediate binding affinity; however, < 5000 nM is related low binding affinity of epitopes
134 towards MHC-II [18, 22, 24].

135 2.4. Prediction of linear B-cell epitopes

136 B-lymphocyte epitopes which are essential for the humoral immune system and antibody
137 production were predicted using the ABCpred server
138 (https://webs.iiitd.edu.in/raghava/abcpred/ABC_submission.html) and neural network algorithm
139 with a length of 16 amino acids and cut-of binding score > 0.51 (0.51 threshold) was used to predict
140 linear B cell epitopes of OmpA, OmpC and OmpF proteins using their consensus sequences. With
141 these criteria, epitopes with higher scores were chosen for the vaccine construction [18, 19]. Also,
142 the linear B-cells epitopes were further subjected to antigenicity prediction using antigen sequence
143 properties tool provided by IEDB website (http://tools.iedb.org/bcell/result/)

144 2.5. Prediction of antigenicity, allergenicity and toxicity

145 The VaxiJen v2.0 server (http://www.ddg-pharmfac.net/vaxijen/VaxiJen/VaxiJen.html)
146 was used to assess the antigenicity of each predicted MHC-I, MHC-II and linear B-Cell epitopes
147 and the multi-epitope vaccine sequence when constructed. The server threshold was set as 0.4 for
148 bacteria. This server utilizes the ACC (auto and cross-covariance) to produce an output [25, 26,
149 27]. To assess whether determined epitopes will cause an allergic reaction or not, the AllerTOP
150 v2.0 server (http://www.ddg-pharmfac.net/AllerTOP) was utilized [28, 29]. The AllerTOP uses
151 the ACC transformation of the protein sequence to obtain the closest k value and compare the E
152 descriptors of amino acids [30]. The ToxinPred server
153 (https://webs.iiitd.edu.in/raghava/toxinpred/multi_submit.php) was used to check the toxicity of
154 all selected epitopes [23, 26]. Following the final construction of the study MEV similar analyses
155 was performed.

156 2.6. Interferon gamma (IFN-γ) inducing epitope prediction

157 The presence of IFN-γ inducing epitopes in the proposed multi-epitope vaccine peptide
158 was predicted by IFNepitope server (http://crdd.osdd.net/raghava/ifnepitope/index.php) using the

159 scan module. Among algorithms models available, the motif and support vector machine (SVM)
160 hybrid model was selected. The server generates all possible overlapping peptides from antigen,
161 based on either IFN-γ inducing and IFN-γ non-inducing datasets [31]. Prediction score >1.0 was
162 set as a threshold value for epitope selection. Considering that IFNepitope server is trained with
163 MHC II epitopes, all final MHC II epitopes selected before chimera assembly was submitted [32].

164 2.7. Epitope conservancy analysis.

165 The prediction of conservation across epitopes was predicted using the IEDB tools
166 (http://tools.iedb.org/conservancy/). Epitope sequences with their corresponding OMP protein
167 class was entered into their respective text area. The minimum conservancy sequence identity
168 threshold was set at >= 100 % [33].

169 2.8. Population coverage analysis

170 The IEDB's Population Coverage tool (http://tools.iedb.org/population/) was used to look
171 at how the affinity of CTL and HTL epitopes for HLA alleles varies by race, location, and country,
172 affecting the construction of epitope-based vaccines. By keeping the default parameters, the 16
173 geographical areas was selected for population coverage. The distribution of human MHC binding
174 alleles was used in this tool to estimate population coverage for the T-cell epitopes, queried by
175 area, country and ethnicity in different parts across the globe [23].

176 2.9. Construction of multi-epitope vaccine sequence

177 For the final multi-epitope vaccine construction, highly antigenic, non-allergenic and non-
178 toxic epitopes were chosen. The Selected B cell epitopes (OmpA, OmpC and OmpF) and HTL
179 epitopes were linked by GPGPG linker and CTL epitopes by an AAY linker. To further enhance
180 the immunogenicity of the multi-epitope vaccine, an adjuvant flagellin (*fliC*) protein (GenBank

181 accession number KAA0422324.1) of *Salmonella enterica* subsp. *enterica* serovar Typhimurium
182 was added through the EAAAK linker at the N terminal of the epitopes [18, 34, 35].

183 2.10. Prediction of physicochemical characteristics and solubility

184 The MEV construct was subjected to Expasy Protparam online server
185 (https://web.expasy.org/protparam/) to predict the physicochemical characteristics of the multi
186 peptide structure such as the aliphatic index, molecular weight (MW), theoretical isoelectric point
187 (pI) [36], half-life, instability, and grand average of hydropathicity (GRAVY) [37]. The Protein-
188 Sol server (http://protein-sol.manchester.ac.uk) was used to determine the solubility value of the
189 multi-epitope vaccine. A scaled solubility value of more than 0.45 indicates that the protein is more
190 soluble than that of the average soluble *E. coli* protein in the experimental solubility dataset.
191 Proteins of lesser scaled solubility value are expected to be insoluble [38].

192 2.11. Secondary structure prediction

193 The secondary structure of the MEV construct was generated using PSIPRED and SOPMA
194 Property online tool, PSIPRED (http://bioinf.cs.ucl.ac.uk/psipred/) is a simple online secondary
195 structure prediction tool that incorporates two feed-forward neural networks which predict
196 transmembrane topology, transmembrane helix, folds, and domains efficiently [39], while the
197 SOPMA server (https://npsa.lyon.inserm.fr/cgi-
198 bin/npsa_automat.pl?page=/NPSA/npsa_sopma.html) is an online tool used to indicate the
199 properties of the secondary structure. This method correctly predicts 69.5% of secondary structure
200 property (alpha-helix, beta-sheet, and coil) in proteins database. The combination of SOPMA and
201 a neural networks method predicts 82.2% of residues for 74% of co-predicted amino acids [40].

202 2.12. Tertiary structure prediction

Iterative Threading Assembly Refinement (I-TASSER) server (https://zhanglab.ccmb.med. Umich.Edu/I-TASSER) was used to create a three-dimensional (3D) structure of the vaccine construct. Based on the sequence-to-structure-to-function paradigm, I-TASSER generates three-dimensional (3D) atomic models from multiple threading alignments and iterative structural assembly simulations. The accuracy of the 3D model is provided based on the confidence score (C-score). The C-score is generally in the range between − 5 and 2, wherein a higher number indicates better quality [32, 41].

2.13. Refinement and validation of tertiary structure

Validation of the tertiary structure is important in vaccine development because it reveals possible flaws in the anticipated model [42]. To improve the quality of 3D structure, refinement of the vaccine model was carried out with the Galaxy Refine web server (http://galaxy.seoklab.org/cgi-bin/submit.cgi?type=REFINE). GalaxyRefne server is premised on a sophisticated routine that accomplishes reassembling and uses molecular dynamics modulation for structural refinement [43]. Furthermore, the ProSA-webserver was used to evaluate the total quality score of the precise input structure for 3D structure validation. ERRAT (http://services.mbi.ucla.edu/ERRAT/) was used to evaluate un-bonded inter-atomic interactions and high-resolution crystallography structures [44, 45]. To validate the refined tertiary structure of the vaccine model, the PROCHECK server (https://saves.mbi.ucla.edu) and VADAR version 1.8 (http://vadar.wishartlab.com/index.html?) was used [46]. The result of these servers is the Ramachandran plot, which shows the percentage of residues in favored, allowed and disallowed regions based on dihedral angles psi (ψ) and phi (φ) of each amino acid [47].

2.14. Prediction of discontinuous B-cell epitopes

225 Protein folding can put distant residues together and generate discontinuous B-cell epitopes.
226 Discontinuous epitopes are predicted using the PI (Protrusion Index) value, and their clustering is
227 based on the distance R (distance between the Centre of mass of the residue), which is measured.
228 A higher R value suggests that there are a greater number of expected discontinuous epitopes.
229 Since more than 90% of B cell epitopes are discontinuous, the presence of these epitopes in the
230 vaccine structure was predicted by the Ellipro server (http://tools.iedb.org/ellipro/) [23, 48]. The
231 threshold parameters (Minimum residue score 0.5 and Maximum distance 6 A) was set at default.
232 Based on the 3D structure of the vaccine, this server provides an ellipsoid score to each residue,
233 which is defined as a PI value. A score of 0.9 PI implies that 90% of the protein's residues are
234 included, while the remaining 10% are outside of the ellipsoid. This PI number is determined by
235 the centre of mass of each residue, which is located outside of the greatest feasible ellipsoid [23,
236 27].

237 2.15. Protein–protein docking

238 The vaccine model is expected to bind to immunological receptors in order to elicit an
239 immune response. Toll-Like Receptor (TLR); TLR-1, TLR-2, TLR-4 and TLR-5 are involved in
240 the recognition of *Salmonella* structures and the production of inflammatory cytokines as they are
241 highly sensitive to bacterial components; TLR-1 (triacylated lipoproteins), TLR-2 (lipoproteins),
242 TLR-4 (lipopolysaccharide) and TLR-5 (flagellin) [49, 50, 51] and so was selected for docking.
243 The potential of chimeric vaccine construct docking with Toll-Like Receptor (TLR) was evaluated
244 by ClusPro 2.0 server (https://cluspro.bu.edu/login.php). ClusPro 2.0 is a rigid-body protein–
245 protein docking service that predicts interactions between two proteins. This software is entirely
246 automated and employs 3 distinct procedures: the first is a unique fast Fourier transform (FFT)
247 correlation, the second is clustering the best energy conformations, and the third is evaluating

248 cluster stability using brief Monte Carlo simulations [52, 53]. The PDB file of the refined vaccine
249 construct was docked against TLR-1 (PDB Id: 6NIH), TLR-2 (PDB ID: 6NIG), TLR-4 (PDB ID:
250 3FXI) and TLR-5 (PDB ID: 3JOA) from the PDB database (https://www.rcsb.org/). The best-
251 docked model was chosen from the models on the ClusPro 2.0 server based on its lowest energy
252 value.

253 2.16. Molecular dynamic simulation and protein-protein binding 254 affinity analysis

255 To investigate the stability and physical movements of the MEV-TLR-1, MEV-TLR-2, MEV-
256 TLR-4 and MEV-TLR-5 docked complexes, molecular dynamics simulation by iMOD server
257 (iMODS) (http://imods.chaconlab.org) was done. This tool explores normal mode analysis (NMA)
258 in internal (dihedral) coordinates that naturally reproduce the joint functional motions of biological
259 macromolecules and generates feasible transition pathways between two homologous structures,
260 even with large macromolecules [54]. The binding affinity and dissociation constant of the docked
261 proteins was predicted by Prodigy, a web-server for predicting the binding affinity in protein-
262 protein complexes (https://wenmr.science.uu.nl/prodigy/), all parameters were set at default [55,
263 56, 57].

264 2.17. Immune simulation

265 The vaccine amino acid sequence were submitted to C-ImmSim server
266 (https://kraken.iac.rm.cnr.it/C-IMMSIM/) in order to determine the immune response profile in
267 the *in-silico* model. C-ImmSim server evaluates humoral and cellular response to vaccine model
268 [58] based on Position-specific scoring matrix (PSSM) and machine learning methods. PSSM
269 stimulates three different anatomical regions of mammals, including Bone marrow (where the

270 hematopoietic stem cells are stimulated, and myeloid cells produced), the thymus (where naive T
271 cells are selected to avoid autoimmunity), and tertiary lymphatic organs to define the real-life
272 immune response. To conduct immune stimulation, the number of antigen to inject was set at 462,
273 three shots was injected at four weeks interval i.e., at days 0, 28 and 56, so the time steps of
274 injections was set at 1, 84, and 168 for each injection number; meaning that each time step is 8
275 hours and time step 1 is the injection administered at time zero. This prime-booster-booster
276 approach at 4-weeks interval was employed to achieve long-lasting protective immune response,
277 and was administrated with a total of 336 simulation steps while all other simulation parameters
278 were set as default [19, 59].

279 2.18. Codon adaptation

280 Efficacy of the vaccine model in cloning and expression is important for *in-vitro* production.
281 Codon adaptation and in silico cloning were performed in order to express the final vaccine
282 construct in a mammalian host since codon usage optimization demonstrated differences between
283 mammals and *Salmonella enterica* strains. The purpose of this is to guarantee the expression of
284 the vaccine construct in the selected host. Java Codon Adaptation Tool (JCAT) server
285 (http://www.prodoric.de/JCat) was used for the reverse translation of the protein sequence of the
286 vaccine construct into DNA sequence. The rho independent transcription termination, prokaryote
287 ribosome binding site and cleavage site of restriction enzyme were avoided [60]. In the JCAT,
288 codon adaptation index (CAI) score is 1.0 but > 0.8 is considered a good score and the favourable
289 GC content of a sequence should range between 30 % and 70 %.

290 2.19. Restriction enzyme mapping and *in-silico* cloning into plasmid

291 The NEBcutter Version 3.0.17 server software (https://nc3.neb.com/NEBcutter/) was used to
292 map out the restriction enzymes on the JCAT codon optimized sequence of the vaccine construct.

293 NEBcutter v3.0 was designed to assist users with restriction digestions and traditional molecular
294 cloning workflows. Users can submit a sequence of interest or select from a list of common
295 plasmids and example sequences. Users can then visualize detected restriction enzyme sites on a
296 sequence map and perform a custom digest with selected enzymes. The restriction enzymes cutting
297 sites sequences of HindIII and BamHI was introduced to the DNA sequence obtained by (JCAT)
298 server at the N-terminal and C-terminal vicinities respectively. A hexa histidine-tag, (6xHis-tag)
299 was inserted into the DNA sequence before BamHI at the C-terminal. The SnapGene restriction
300 cloning module was used to insert the DNA sequence into pcDNA3.1_CT-GFP expression vector
301 (https://www.snapgene.com/plasmids/mammalian_expression_vectors/pcDNA3.1_CT-GFP)
302 within the multiple cloning sites of the plasmid. The pcDNA3.1_CT-GFP expression plasmid
303 vector which is mammalian codon optimized for transfection visualization in mammalian cell line
304 was chosen [44, 60, 61].

305 3.0. Results

306 3.1. Retrieval of *S.* Kentucky OMP sequences and generation of 307 consensus sequence

308 *Salmonella* Kentucky Omps A, C and F sequences and their accession number were
309 obtained from the NCBI protein database as FASTA files. A total of 65 outer membrane proteins
310 (Omps) of *Salmonella* Kentucky were retrieved, comprising of 18 OmpA, 32 OmpC and 15 OmpF.
311 The FASTA format sequences of all 65 OMPs A, C and F class were aligned separately by Jalview
312 2.11.2.7. The FASTA sequence of *fliC* protein (GenBank accession number KAA0422324.1) of
313 *Salmonella* Typhimurium used as Adjuvant was also retrieved (Table 2).

314 **Table 1. Accession number of the outer membrane proteins A, C and F selected for the**

315 **development of MEV retrieved from NCBI protein database.**

S/No.	OmpA	OmpC	OmpF
1	ELX43285.1	EDX45415.1	CAH2847802.1
2	EDZ19256.1	EDZ22335.1	CAH2871873.1
3	EDX48073.1	CAH2866635.1	ESG84125.1
4	EJQ7725175.1	CAH2866410.1	ESG88044.1
5	EDF7307973.1	ERN84404.1	ESC06125.1
6	EJW1777139.1	ERN77197.1	ELX43265.1
7	EBL3626682.1	ERN70439.1	ERN84743.1
8	ECV5604453.1	ERN69676.1	ERN79626.1
9	EBM7532700.1	ERN69269.1	ERN78365.1
10	EFL6925197.1	ESG79344.1	ERN73560.1
11	EBW8725894.1	ESG77524.1	ERN62106.1
12	ECI8791934.1	ESC11174.1	EDZ19170.1
13	EGC5146150.1	ELX37395.1	EDX44525.1
14	ESG79962.1	ERN88917.1	EJC3163576.1
15	ESG88025.1	ERN87695.1	EBL4572010.1
16	ESC13401.1	ERN87644.1	
17	CAH2847702.1	ERN82780.1	
18	CAH2871911.1	ERN77612.1	
19		ERN77081.1	
20		ERN76635.1	

21		ERN74999.1	
22		ERN72553.1	
23		ERN70652.1	
24		ERN69005.1	
25		ERN68685.1	
26		ERN67044.1	
27		ERN66706.1	
28		ERN66672.1	
29		ERN66415.1	
30		ERN64040.1	
31		ERN62720.1	
32		ERN62687.1	

316 **Table 2**. **Jalview version 2.11.2.7 generated consensus sequences of the outer membrane**

317 **proteins A, C and F and selected *fliC* protein for the development of MEV.**

Proteins	**FASTA sequences/number of amino acids**
OmpA	>Consensus sequence comprising 371 amino acid residues

	MKKTAIAIAVALAGFATVAQAAPKDNTWYAGAKLGWSQYHDTGFINND GPTHENQLGAGAFGGYQVNPYVGFEMGYDWLGRMPYKGDNINGAYKA QGVQLTAKLGYPITDDLDVYTRLGGMVWRADTKSNVPGPGGASNKDHD TGVSPVFAGGIEYAITPEIATRLEYQWTNNIGDANTIGTRPDNGLLSVGVS YRFGQQEAAPVVAPAPAPAPEVQTKHFTLKSDVLFNFNKSTLKPEGQQAL DQLYSQLSNLDPKDGSVVVLGFTDRIGSDAYNQGLSEKRAQSVVDYLISK GIPSDKISARGMGESNPVTGNTCDNVKPRAALIDCLAPDRRVEIEVKGVKD VVTQPQARRVEIEVKGVKDVVTQPQA
OmpC	>Consensus sequence comprising 403 amino acid residues
	MKVKVLALLVPALLVAGAANAAEIYNKDGNKLDLYGKVDGLHYFSDDK GSDGDQTYMRIGFKGETQINDQLTGYGQWEYQIQGNQTEGSGDSSTRVA FAGLLFFDAGSFDDGGNYGVTYDVTSWTDVLPEFGGGTYGADNFMQQR GNGYATYRNTDFFGFVDGLDFALQYQGKNGSVSGENTNGRSGLNQNGD GYGGSLTYAIGEGFSVGGAITTSKRTADQNNTANDRLYGNGDRATVYTG GLKYDANNIYLAAQYSQTYNAARFGTSNGSTPSTSYGFANKAQNFEVVA QYQFDFGLRPSVAYLQSKGKDISNGGGASYGDQDIVKYVDVGATYYFNK NMSTYVDYKINLLDKNDFTRDAGINTDDIVALGLVYQFIVALGMVYQFIA TDDIVGVGLVYQF
OmpF	>Consensus sequence comprising 363 amino acid residues

	MMKRKILAAVIPALLAAATANAAEIYNKDGNKLDLYGKAVGRHVWTTTGDSKNADQTYAQIGFKGETQINTDLTGFGQWEYRTKADRAEGEQQNSNLVRLAFAGLKYAEVGSIDYGRNYGIVYDVESYTDMAPYFSGETWGGAYTDNYMTSRAGGLLTYRNSDFFGLVDGLSFGIQYQGKNQDNHSINSQNGDGVGYTMAYEFDGFGVTAAYSNSKRTNDQQDRDGNGDRAESWAVGAKYDANNVYLAAVYAETRNMSIVENTVTDTVEMANKTQNLEVVAQYQFDFGLRPAISYVQSKGKQLNGADGSADLAKYIQAGATYYFNKNMNVWVDYRFNLLDENDYSSSYVGTDDQAAVGITYQF
fliC	49 amino acid residues
	MAQVINTNSLSLLTQNNLNKSQSALGTAIERLSSGLRINSAKDDAAGQA

3.2. Results for MHC-I and MHC-II epitopes prediction and epitope conservancy analysis

At a threshold value of 0.5 percent for strong binders and following antigenicity, allergenicity and toxicity screening, a final total of 4 CTL epitopes for OmpA, 5 CTL epitopes for OmpC and 5 CTL epitopes for OmpF which were selected for the multi-epitope vaccine construction (Table 3). Their corresponding allele(s) and positions were noted (Table 4). The result from IEDB server using the seven-allele reference set and applicable thresholds generated 4, 2 and 2 HTL epitopes were selected for OmpA, OmpC and OmpF respectively which were selected for the construction of the multi-epitope vaccine (Table 3). Their corresponding allele(s) and positions were noted (Table 4). Also, the results from IEDB server conservancy analysis at > = 100 % protein sequence identity threshold predicted a minimum and maximum identity of 100 % for all epitopes across the different classes of OMPs A, C and F CTLs and HTLs. Epitope “IEYAITPEI” had a

330 100 % minimum and maximum identity conservancy as an OmpA, but had a minimum identity at
331 33.33 % and a maximum identity at 33.33 % as an OmpC CTL epitope (Table 4).

332 **Table 3. Predicted CTL and HTL epitopes of *S.* Kentucky OmpA, OmpC and OmpF proteins**
333 **from consensus sequences with their immunogenic properties**

Epitopes	Peptide Score	Antigenicity (Score)	Allergenicity	Toxicity
LSVGVSYRF	0.93	Antigenic (1.5084)	Non-Allergen	Non-Toxin
EVQTKHFTL	0.91	Antigenic (1.5694)	Non-Allergen	Non-Toxin
IEYAITPEI	0.81	Antigenic (1.2128)	Non-Allergen	Non-Toxin
VQLTAKLGY	0.84	Antigenic (0.7491)	Non-Allergen	Non-Toxin
FNFNKSTLK	0.74	Antigenic (0.6346)	Non-Allergen	Non-Toxin
YKGDNINGA	0.59	Antigenic (1.2899)	Non-Allergen	Non-Toxin
LAPDRRVEI	0.89	Antigenic (0.5152)	Non-Allergen	Non-Toxin
VALGLVYQF	0.91	Antigenic (0.8219)	Non-Allergen	Non-Toxin

GLRPSVAYL	0.87	Antigenic (0.9049)	Non-Allergen	Non-Toxin
LPEFGGGTY	0.89	Antigenic (0.8301)	Non-Allergen	Non-Toxin
ISNGGGASY	0.82	Antigenic (1.5949)	Non-Allergen	Non-Toxin
RGNGYATYR	0.80	Antigenic (1.0838)	Non-Allergen	Non-Toxin
FNKNMSTYV	0.82	Antigenic (1.1373)	Non-Allergen	Non-Toxin
MSTYVDYKI	0.81	Antigenic (1.0144)	Non-Allergen	Non-Toxin
SQNGDGVGY	0.93	Antigenic (2.5198)	Non-Allergen	Non-Toxin
DENDYSSSY	0.92	Antigenic (0.6581)	Non-Allergen	Non-Toxin
AAVGITYQF	0.84	Antigenic (1.2698)	Non-Allergen	Non-Toxin
IQAGATYYF	0.87	Antigenic (0.6830)	Non-Allergen	Non-Toxin
TAAYSNSKR	0.91	Antigenic (0.4845)	Non-Allergen	Non-Toxin

YYFNKNMNV	0.93	Antigenic (0.8472)	Non-Allergen	Non-Toxin
YAETRNMSI	0.91	Antigenic (0.9418)	Non-Allergen	Non-Toxin

335 **Table 4. The predicted MHC restricted allele(s) of the CTL and HTL epitopes and degree of conservancy for the OMPs A, C**

336 **and F screened for antigenicity, allergenicity and toxicity**

Omps	MHCI Epitopes	MHCII Epitopes	MHC Restricted Allele(s)	Start	End	Percent of protein sequence matches at identity <= 100%	Minimum identity	Maximum identity
OmpA	LSVGVSYRF		HLA-B*58:01, HLA-B*57:01	117	125	100.00% (1/1)	100.00%	100.00%
	EVQTKHFTL		HLA-B*08:01	143	151	100.00% (1/1)	100.00%	100.00%
	IEYAITPEI		HLA-B*40:01	82	90	100.00% (1/1)	100.00%	100.00%
	VQLTAKLGY		HLA-B*15:01, HLA-A*30:02	26	34	100.00% (1/1)	100.00%	100.00%
		FNFNKSTLK	HLA-DRB3*02:02, HLA-DRB5*01:01	152	168	100.00% (1/1)	100.00%	100.00%
		YKGDNINGA	HLA-DRB3*01:01,	9	23	100.00% (1/1)	100.00%	100.00%

			HLA-DRB3*02:02					
		LAPDRRVEI	HLA-DRB1*03:01	254	270	100.00% (1/1)	100.00%	100.00%
		IEYAITPEI	HLA-DRB1*07:01	79	93	100.00% (1/1)	100.00%	100.00%
OmpC	VALGLVYQF		HLA-B*57:01, HLA-B*58:01, HLA-B*53:01, HLA-B*35:01	298	306	100.00% (1/1)	100.00%	100.00%
	IEYAITPEI		HLA-DRB1*07:01	79	93	0.00% (0/1)	33.33%	33.33%
	GLRPSVAYL		HLA-A*02:03, HLA-A*02:01	226	234	100.00% (1/1)	100.00%	100.00%
	LPEFGGGTY		HLA-B*35:01	56	64	100.00% (1/1)	100.00%	100.00%
	ISNGGGASY		HLA-B*15:01, HLA-A*30:02, HLA-A*01:01, HLA-B*35:01	241	249	100.00% (1/1)	100.00%	100.00%
	RGNGYATYR		HLA-A*31:01	73	81	100.00% (1/1)	100.00%	100.00%

		FNKNMSTYV	HLA-DRB3*02:02	263	278	100.00% (1/1)	100.00%	100.00%
		MSTYVDYKI	HLA-DRB1*15:01	265	281	100.00% (1/1)	100.00%	100.00%
OmpF	SQNGDGVGY		HLA-B*15:01, HLA-A*30:02	117	125	100.00% (1/1)	100.00%	100.00%
	DENDYSSSY		HLA-B*44:03, HLA-B*44:02	268	276	100.00% (1/1)	100.00%	100.00%
	AAVGITYQF		HLA-B*58:01, HLA-B*57:01, HLA-B*35:01, HLA-A*32:01	283	291	100.00% (1/1)	100.00%	100.00%
	IQAGATYYF		HLA-A*23:01, HLA-A*24:02, HLA-B*15:01	244	252	100.00% (1/1)	100.00%	100.00%
	TAAYSNSKR		HLA-A*68:01	137	145	100.00% (1/1)	100.00%	100.00%

		YYFNKNMNV	HLA-DRB3*02:02	244	262	100.00% (1/1)	100.00%	100.00%
		YAETRNMSI	HLA-DRB1*07:01	174	190	100.00% (1/1)	100.00%	100.00%

338 ## 3.3. Linear B-cell epitopes prediction

339 ABCpred server predicted a total of 35 B-cell epitopes for the consensus sequence of
340 OmpA, 39 B-cell epitopes for the consensus sequence of OmpC and 41 B-cell epitopes for the
341 consensus sequence of OmpF with a cut off binding score at 0.51. B-cell epitopes with a high score
342 of ≥ 0.85 and a minimum peptide rank score of 7 were further subjected to antigenicity,
343 allergenicity and toxicity screening. Finally, 2 B-cell epitopes for OmpA, 2 B-cell epitopes for
344 OmpC and 3 B-cell epitopes for OmpF were selected for multi-epitope vaccine construction (Table
345 5).

346 **Table 5. Predicted linear B-cells epitopes of *S*. Kentucky OMP A, C and F from consensus sequences and *flic* protein (adjuvant)**

347 **with their immunogenic properties**

OMPs	**B-cell Epitopes (16mers)**	**Average K and T score**	**Peptide score**	**Antigenicity (Score)**	**Allergenicity**	**Toxicity**
OmpA	DYLISKGIPSDKISAR	1.020	0.89	Antigenic (0.8497)	Non-Allergen	Non-Toxin
	GPGGASNKDHDTGVSP	0.953	0.88	Antigenic (1.7585)	Non-Allergen	Non-Toxin
OmpC	TSNGSTPSTSYGFANK	0.980	0.90	Antigenic (0.8885)	Non-Allergen	Non-Toxin
	AGAANAAEIYNKDGNK	0.971	0.89	Antigenic (1.2510)	Non-Allergen	Non-Toxin
OmpF	VGRHVWTTTGDSKNAD	0.956	0.92	Antigenic (1.4812)	Non-Allergen	Non-Toxin

	GFGVTAAYSNSKRTND	0.994	0.90	Antigenic (1.2497)	Non-Allergen	Non-Toxin
	DGLSFGIQYQGKNQDN	1.001	0.89	Antigenic (1.1403)	Non-Allergen	Non-Toxin
Flic	GenBank accession number KAA0422324.1			Antigenic (0.7058)	Non-Allergen	Non-Toxin

348 Key: **K and T**: Kolaskar and Tongaonkar antigenicity scale

3.4. Interferon gamma (IFN-γ) inducing epitope prediction

Eight MHC class II epitopes were submitted to the IFNepitope server for IFN-γ prediction. Two HTL epitopes were positive, thus; capable of inducing the production of interferon gamma. The SVM method predicted epitope "LAPDRRVEI" as a positive inducer and the MERCI method predicted "IEYAITPEI" epitope as a positive inducer (Table 6).

Table 6. Predicted OMPs A, C and F MHC Class II T-cell epitopes capable of inducing interferon gamma (IFN-γ)

Epitope 15 length Peptide	Epitope Sequence	Method	Result	Score
DVLFNFNKSTLKPEG	FNFNKSTLK	SVM	NEGATIVE	-0.3144975
RMPYKGDNINGAYKA	YKGDNINGA	SVM	NEGATIVE	-0.073986311
IDCLAPDRRVEIEVK	LAPDRRVEI	SVM	POSITVE	-0.053153702
AGGIEYAITPEIATR	IEYAITPEI	MERCI	POSITVE	1
FNKNMSTYVDYKINL	FNKNMSTYV	SVM	NEGATIVE	-0.96274966
FNKNMSTYVDYKINL	MSTYVDYKI	MERCI	NEGATIVE	1
GATYYFNKNMNVWVD	YYFNKNMNV	SVM	NEGATIVE	-0.62234638
AAVYAETRNMSIVEN	YAETRNMSI	SVM	NEGATIVE	-0.55036682

3.5. Population coverage

The worldwide population percentage coverage of the selected putative HLA class I and HLA class II restricted epitopes was 94.91 %. This analysis of the MHC I and MHC II alleles confirmed that the world population will be covered if the intended vaccine architecture was administered. Based on continental and regional analysis, Europe, North America and North Africa had the

361 highest population coverage of 97.59 %, 96.92 % and 92.89 % respectively (Fig 1). On the African
362 continent, the percentage population coverage for West Africa, South Africa, East Africa and
363 Central Africa were 89.77 %, 83.02 %, 81.86 % and 78.17 % respectively with a class combined
364 regional average of 85.14 (Table 7). Outside the African continent, East Asia, North-East Asia and
365 South America were 90.82 %, 79.71 % and 83.0 % respectively (Fig 1). Furthermore the selected
366 putative HLA class I restricted epitopes exhibited a higher individual percentage coverage (90.02
367 %) when queried against the HLA class II restricted epitopes (49.02 %) across the world (Fig 1).
368 **Fig 1. Continental and regional coverage of the MHC class I and MHC class II T-Cell**
369 **epitopes**

370 **Table 7. Percentage population Coverage of MHC class I and MHC class II epitopes in different regions in Africa**

Population/ Area	Class I			Class II			Class combined		
	Coverage[a]	Average hit[b]	pc90[c]	Coverage[a]	Average hit[b]	pc90[c]	Coverage[a]	Average hit[b]	pc90[c]
Central Africa	70.01%	1.74	0.33	27.2%	0.42	0.14	78.17%	2.16	0.46
East Africa	76.69%	1.88	0.43	22.21%	0.32	0.13	81.86%	2.2	0.55
North Africa	85.1%	2.09	0.67	52.24%	0.84	0.21	92.89%	2.93	1.14
South Africa	77.2%	1.86	0.44	25.52%	0.26	0.13	83.02%	2.12	0.59
West Africa	86.84%	2.61	0.76	22.25%	0.32	0.13	89.77%	2.93	0.98
Average	79.17	2.04	0.53	29.88	0.43	0.15	85.14	2.47	0.74
Standard deviation	6.13	0.31	0.16	11.34	0.21	0.03	5.39	0.38	0.27

371 **Key**

372 [a] projected population coverage

373 [b] average number of epitope hits / HLA combinations recognized by the population

374 [c] minimum number of epitope hits / HLA combinations recognized by 90% of the population

375 ## 3.6. Construction of MEV sequence and interferon gamma (IFN-γ)
376 ## induction capabilities of the MEV

377 The multi-epitope vaccine construct consists of 462 amino acids residues from a total of
378 28 selected antigenic T-cells and B-cell epitopes comprising 14 CTLS, 7 HTLs and 7 B-cell
379 epitopes, covalently linked to an immuno-adjuvant (*Salmonella* Typhimurium *fliC* protein;
380 GenBank accession number KAA0422324.1 with 49 amino acid residues). The *fliC* protein was
381 fused to the epitopes of CTLs with an EAAAK linker at the N terminal end of the vaccine
382 construct. The CTL peptides of OmpA, OmpC and OmpF were fused together with an AAY linker
383 and fused to the first HTL OmpA epitope with an AAY linker. The HTL peptides and B-cell
384 epitopes were fused together with a GPGPG linker with the B-cell epitope of OmpF at the C
385 terminal end (Fig 2). Result of antigenicity, allergenicity and toxicity prediction on the MEV
386 construct confirms the vaccine as antigenic (with a score of 1.0458), non-allergenic and non-toxin.

387 The IFNepitope server support vector machine (SVM) hybrid model result confirmed a positive
388 result capable of inducing IFN-γ and a score of 1.5695871.

389 **Fig 2. The schematic structural arrangement of the final multi-epitope vaccine construct**

390 ## 3.7. Prediction of physicochemical characteristics and solubility of the
391 ## MEV

392 The physicochemical parameters and solubility properties of the chimeric vaccine
393 construct using Expasy Protparam and the Protein-Sol servers expressed the following. The
394 molecular weight of the vaccine construct was 47343.98 Da and the bio-computed theoretical
395 isoelectric point (pI) was 9.150. The estimated half-life in mammalian cell is 30 hours, >20 hours
396 and >10 hours yeast and *Escherichia coli* respectively. The solubility of the vaccine was found to

397 be 0.452 on the protein sol server (value > 0.45 is predicted to have a higher solubility than the
398 average soluble *E. coli* protein). The instability index of the vaccine was 25.66, signifying that the
399 vaccine is stable in a solvent environment (> 40 signifies instability). The aliphatic index was
400 computed to be 57.23 (The aliphatic index of a protein is a measure of the relative volume occupied
401 by aliphatic side chain of the following amino acids: alanine, valine, leucine and isoleucine. An
402 increase in the aliphatic index increases the thermo stability of globular proteins). The GRAVY
403 score was -0.429, which infers that the vaccine proteins have better interactions with water
404 molecules (To measure the hydrophobic and hydrophilic properties of the protein, general average
405 hydropathicity (GRAVY) score is a widely used parameter in codon usage bias (CUB) analysis
406 and its value ranges from −2 to 2. Positive GRAVY score means the protein is hydrophobic, while
407 negative GRAVY score indicates a hydrophilic protein).

408 3.8. Prediction of secondary and tertiary structure

409 Result for secondary structure analysis of the designed multi-epitope vaccine from
410 PSIPRED and SOPMA server indicated that 77 amino acids (16.67 %) were alpha-helices, 41
411 amino acids (8.87 %) were extended beta strands, 21 amino acids (4.55 %) were beta turns, and
412 323 amino acid (69.91 %) were random coils (Fig 3).
413 The 3D structure was built by I-Tasser server. According to the threading templates, 5 tertiary 3D
414 structures was predicted. The best C-score model with a -0.69 C-score value was selected for
415 further refinement and validation. The consistency of the 3D model was improved by galaxy refine
416 web server. Five improved refined models were produced from the initial MEV model (the -0.69
417 C-score structure from I-Tasser). Model 2 was the most significant model based on the
418 computational structural qualities. Model 2 had a GDT-HA score of 0.9221, RMSD of 0.493,

419 MolProbity of 2.352, a Clash score of 13.7, a zero Poor rotamers (0.0) and Rama favoured value
420 of 82.0 (Fig 4).
421 The validation of the refined tertiary structure of the MEV on the PROCHECK and VADAR
422 version 1.8 servers produced a Ramachandran plot with 264 number of the residues (75.6 %) in
423 the most favored region, 57 number of residues (16.3%) in additional allowed regions, 19 number
424 of residues (5.4 %) in generously allowed regions and 9 number of residues (2.6 %) in the
425 disallowed regions, making a total of 349 number of non-glycine and non-proline residues.
426 Additionally, there were 77 number of glycine residues, 34 number of proline residues and 2
427 number of end-residues (excl. Gly and Pro) (Fig 5).

428 **Fig 3. The PSIPRED and SOPMA server graphical demonstration of secondary structure**
429 **properties of the final designed MEV**

430 **Fig 4. The tertiary structure of the designed MEV predicted by I-TASSER and coloured with**
431 **ChimeraX software.** *fliC* protein (adjuvant) coloured in Red, CTLs in Purple, HTLs in Blue and
432 B-cell epitopes in Lime green

433 **Fig 5. Validation:** Ramachandran plot analysis of protein residues, showing 75.6 % in favored,
434 21.7 % in allowed, and 2.6 % in disallowed regions

435 3.9. Predicted discontinuous B-cell epitopes

436 The prediction of discontinuous epitopes requires the 3D structural information of the
437 protein or polypeptide. Thus, ElliPro server was used to predict three discontinuous B-cell
438 epitopes for the MEV indicating its residues, number of residues and scores (Table 8). The 3D
439 representation of putative B-cell epitopes is shown in Fig 6 with yellow surface.

440 **Table 8. Predicted discontinuous B-cell epitopes residues of the designed MEV, predicted by**

441 **ElliPro**

S/no	Residues	Number of Residues	Score
1	A:M1, A:A2, A:Q3, A:V4, A:I5, A:N6, A:T7, A:N8, A:S9, A:L10, A:S11, A:L12, A:L13, A:T14, A:Q15, A:N16, A:N17, A:L18, A:N19, A:K20, A:S21, A:Q22, A:S23, A:A24, A:L25, A:G26, A:T27, A:A28, A:I29, A:E30, A:R31, A:L32, A:S33, A:S34, A:G35, A:L36, A:R37, A:I38, A:N39, A:S40, A:A41, A:K42, A:D43, A:D44, A:A45, A:A46, A:G47, A:Q48, A:A49, A:E50, A:A51, A:A52, A:A53, A:K54, A:L55, A:S56, A:V57, A:G58, A:V59, A:S60, A:R62	62	0.869

2	A:P235, A:G239, A:N241, A:I242, A:N243, A:G244, A:A245, A:G246, A:P247, A:G248, A:P249, A:P261, A:G262, A:P263, A:G264, A:F265, A:N266, A:K267, A:N268, A:M269, A:S270, A:T271, A:G274, A:P275, A:G276, A:P277, A:G278, A:M279, A:S280, A:Y282, A:V283, A:Y285, A:K286, A:I287, A:G288, A:P289, A:G290, A:P291, A:G292, A:Y294, A:F295, A:N296, A:K297, A:N298, A:M299, A:N300, A:V301, A:G302, A:P303, A:G304, A:P305, A:G306, A:Y307, A:A308, A:E309, A:T310, A:R311, A:N312, A:M313, A:S314, A:I315, A:G316, A:P317, A:G318, A:P319, A:G320, A:D321, A:Y322, A:L323, A:I324, A:S325, A:K326, A:G327, A:I328, A:P329, A:S330, A:D331, A:K332, A:I333, A:S334, A:A335, A:R336, A:G337, A:P338, A:P343, A:G344, A:G345, A:A346, A:S347, A:N348, A:K349, A:D350, A:H351, A:D352, A:T353, A:G354	96	0.681
3	A:A88, A:V91, A:Q92, A:T94, A:A95, A:K96, A:L97, A:G98, A:Y99, A:A100, A:A101, A:Y102, A:V103, A:A104, A:L105, A:G106, A:L107, A:V108, A:Y109, A:Q110, A:F111, A:A112, A:A113, A:Y114, A:G115, A:L116, A:R117, A:P118, A:S119, A:V120, A:Y122, A:L123, A:D175, A:E176, A:N177, A:D178, A:Y179, A:S180, A:S181, A:S182, A:Y183, A:A184, A:A185, A:Y186, A:A187, A:A188, A:V189, A:G190, A:I191, A:T192, A:Y193, A:Q194, A:F195, A:A196, A:A197, A:Y198, A:I199,	100	0.632

	A:Q200, A:A201, A:G202, A:A203, A:T204, A:Y205, A:Y206, A:F207, A:A208, A:H408, A:V409, A:W410, A:T411, A:T412, A:T413, A:G414, A:D415, A:S416, A:K417, A:N418, A:A419, A:D420, A:G421, A:P422, A:G423, A:P424, A:G425, A:G426, A:F427, A:G428, A:V429, A:T430, A:A431, A:A432, A:Y433, A:S436, A:R438, A:N440, A:G442, A:P443, A:D447, A:G448, A:Q456		

443 **Fig 6. 3D representation of the discontinuous B cell epitopes of MEV. The yellow surface**
444 **shows discontinuous B cell epitopes, while grey stick represents the bulk of the polyprotein.**
445 **(a) With 61 number of residues and a score of 0.869, (b) with 96 number of residues with a**
446 **score of 0.681 and (c) with 100 number of residues with a score of 0.632**

447 3.10. Protein–protein docking and protein-protein binding affinity 448 simulation

449 Result from the ClusPro web server provided a protein-protein docking complex with the
450 best model selected based on their lowest energy level score (Table 9). The 3D tertiary structural
451 models of the selected toll-like receptors multi-epitope vaccine docked complexes are on fig 7.
452 ChimeraX software was used for visualization.

453 **Table 9: Result for protein-protein docking on the ClusPro 2.0 server**

Protein-Protein Dock complex	Best model (Cluster)	Center Energy	Lowest Energy
MEV-TLR1	8	-1112.4	-1220.2
MEV-TLR2	7	-1396.7	-1396.7
MEV-TLR4	1	-1002.2	-1213.1
MEV-TLR5	2	-1631.5	-1631.5

455 **Fig 7. The ClusPro protein–protein docking of multi-epitope vaccine (MEV) model with Toll-**
456 **like receptors (TLR).** (a) MEV construct with TLR-1 (PDB Id: 6NIH), (b) MEV construct with
457 TLR-2(PDB ID: 6NIG), (c) MEV construct with TLR-4 (PDB ID: 3FXI) and (d) MEV construct
458 with TLR-5 (PDB ID: 3JOA). All models were visualized and coloured using ChimeraX software

459 3.11. Molecular dynamic simulation and protein-protein binding 460 affinity analysis

461 Molecular dynamic simulation of the TLR-MEV docked complex was executed by
462 iMODs. Results from the iMOD server tool evaluated the stability and physical movements of all
463 the TLR-MEV docked complexes (Fig. 8 to Fig 11). The main-chain deformability is a measure
464 of the capability of a given molecule to deform at each of its residues. The location of the chain
465 'hinges' can be derived from high deformability regions. The B-factor values quantifies the
466 uncertainty of each atom in the complex and is calculated by normal mode analysis and are
467 proportional to Root Mean Square. The eigenvalue of the docked complex, shows the energy
468 required to deform the structure. The eigenvalue for the complexes were 8.6598×10^{-6},
469 3.6955×10^{-7}, 1.6199×10^{-5} and 6.0634×10^{-6} for TLR1-MEV, TLR2-MEV, TLR4-MEV and
470 TLR-MEV respectively. The covariance matrix plot between the pairs of residues, indicates their
471 correlations (red: correlated, white: uncorrelated, blue: anti-correlated). The elastic network model
472 plot suggests the connection between atoms and springs. The springs are more rigid if their greys
473 are darker.
474 For the binding affinity analysis, the Prodigy bioinformatics tool shows a Pearson's
475 Correlation *r* of 0.73 (p-value < 0.0001) between the predicted and the experimental values and a
476 Root Mean Square Error (RMSE) of 1.89 kcal mol^{-1}. Two residues are defined in contact if any of
477 their heavy atom is within a distance of 5.5 Å (Angstrom). The Prodigy server predicted 54 number

478 of intermolecular contacts for MEV-TLR1 complex, 101 number of intermolecular contacts for
479 MEV-TLR2, 168 number of intermolecular contacts for MEV-TLR4 and 50 number of
480 intermolecular contacts for MEV-TLR5. The binding affinity score (ΔG (kcal mol^{-1}) were all
481 negative for all docked complexes predicted (Table 10).

482 **Figure 8. iMODs simulation of TLR1-MEV docked complex**. (a) Main-chain deformability
483 simulation. (b) B-factor values quantifying the uncertainty of each atom. (c) The eigenvalue
484 showing the energy required to deform the structure. (d)The variance associated to each normal
485 mode is inversely related to the eigenvalue. Colored bars show the individual (Purple) and
486 cumulative (green) variances. (e) Covariance matrix indicates coupling between pairs of residues
487 (f) The elastic network model, suggesting the connection between atoms and springs.

488 **Figure 9. iMODs simulation of TLR2-MEV docked complex**. (a) Main-chain deformability
489 simulation. (b) B-factor values quantifying the uncertainty of each atom. (c) The eigenvalue
490 showing the energy required to deform the structure. (d)The variance associated to each normal
491 mode is inversely related to the eigenvalue. Colored bars show the individual (Purple) and
492 cumulative (green) variances. (e) Covariance matrix indicates coupling between pairs of residues
493 (f) The elastic network model, suggesting the connection between atoms and springs.

494 **Figure 10. iMODs simulation of TLR4-MEV docked complex.** (a) Main-chain deformability
495 simulation. (b) B-factor values quantifying the uncertainty of each atom. (c) The eigenvalue
496 showing the energy required to deform the structure. (d)The variance associated to each normal
497 mode is inversely related to the eigenvalue. Colored bars show the individual (Purple) and
498 cumulative (green) variances. (e) Covariance matrix indicates coupling between pairs of residues
499 (f) The elastic network model, suggesting the connection between atoms and springs.

500 **Figure 11. iMODs simulation of TLR5-MEV docked complex.** (a) Main-chain deformability
501 simulation. (b) B-factor values quantifying the uncertainty of each atom. (c) The eigenvalue
502 showing the energy required to deform the structure. (d)The variance associated to each normal
503 mode is inversely related to the eigenvalue. Colored bars show the individual (Purple) and
504 cumulative (green) variances. (e) Covariance matrix indicates coupling between pairs of residues
505 (f) The elastic network model, suggesting the connection between atoms and springs.

506 **Table 10. Prediction of binding Affinity and Dissociation constant**

Protein-protein complex	ΔG (kcal mol^{-1})	K_d (M) at 25℃	ICs charged-charged	ICs charged-polar	ICs charged-apolar	ICs polar-polar	ICs polar-apolar	ICs apolar-apolar	NIS charged	NIS apolar
MEV-TLR1	-10.4	2.3e-08	13	20	9	3	7	2	27.61	26.01
MEV-TLR2	-9.4	1.4e-07	12	12	13	15	14	35	28.08	28.83
MEV-TLR4	-18.1	5e-14	23	33	38	13	36	25	24.81	32.01
MEV-TLR5	-8.8	3.6e-07	3	6	11	0	9	21	19.56	42.13

507 **Key:**

508 **ICs** – Intermolecular Contacts

509 **ΔG** – Binding Affinity (Gibbs free energy)

510 **K_d** – Dissociation constant

511 **NIS** – Non interacting surface

512 ## 3.12. Immune simulation

513 The administration and repetitive exposure to the MEV vaccine elicited a significant
514 increase in the antibody response with a simultaneous decrease in the antigen level over time.
515 There was a significant IgM and IgG humoral response indicating some levels of seroconversion.
516 Humoral responses for both IgM and IgG peaked higher to the booster doses than the prime dose,
517 and IgM was predominantly higher than IgG (and its isotype) (Fig. 12a).

518 Following the administration of the prime dose, CD8+ T-cell and CD4+ responses were actively
519 elicited. The CD4+ T-helper lymphocytes peaked after the second booster, with the active entity
520 state and Th-memory phenotype significantly increased following the first booster and sustained
521 with minimal decay after 100 days (Fig. 13a and Fig. 13b). Similarly, Following the prime dose,
522 there was a highly significant spike in IFN-g response (associated with both CD8+ T-cell and
523 CD4+ Th 1 response), and fairly significant spike in IL-2, IL-10, IL-12 and TGF-b (Transforming
524 growth factor-beta) cytokines response associated with T-reg phenotype (TGF-b and IL-10). These
525 responses were sustained after the two booster doses for IFN-g response and increased
526 significantly for IL-2, IL-10, IL-12 and TGF-b (Fig 15b). These immune readouts are generally
527 associated with a wider base in the spike peak of antigenic quantification.

528 Analysis of B-cell population per cell showed overall B-cell population and B-cell memory
529 responses were higher and stable showing minimal decay. B-cell memory was sufficiently elicited
530 and peaked following the second booster dose and was sustained over 100 days. The same results
531 go for B-cell population per state where active B-cell population was higher and stable for the
532 same number of periods (Fig 12b and Fig 12c). There was also a concomitant increase in dendritic
533 cells and natural killer cells and macrophages activities throughout the duration of the simulation
534 (Fig. 14b, Fig. 14c and Fig. 14d). This points to another good performance indicator of the vaccine

535 construct showing its ability to stimulate the right immunological compartment for effective
536 response. Overall, these results revealed that with each vaccination schedule there was a steady
537 and concomitant increase in immune responses over time.

538 **Fig 12. Distribution of B lymphocytes and their isotypes.** (a) Antigen and immunoglobulins.
539 Antibodies are sub-divided per isotype. (b) B lymphocytes: total count, memory cells, and sub-
540 divided in isotypes IgM, IgG1 and IgG. (c) B lymphocytes population per entity-state (i.e.,
541 showing counts for active, presenting on class-II, internalized the Ag, duplicating and anergic. (d)
542 Plasma B lymphocytes (PLB) count sub-divided per isotype (IgM, IgG1 and IgG2).

543 **Fig 13.** (a) CD4+ T-helper lymphocytes count. The plot shows total and memory counts. (b) CD4+
544 T-helper lymphocytes count sub-divided per entity-state (i.e., active, resting, anergic and
545 duplicating). (c) CD4+ T-regulatory lymphocytes count. Both total, memory and per entity-state
546 counts are plotted here. (d) CD8+ T-cytotoxic lymphocytes count. Total and memory shown

547 **Fig 14.** (a). CD8+ T-cytotoxic lymphocytes count per entity-state. (b) Natural Killer cells (total
548 count). (c) Dendritic cells. DC can present antigenic peptides on both MHC class-I and class-II
549 molecules. The curves show the total number broken down to active, resting, internalized and
550 presenting the ag. (d) Macrophages. Total count, internalized, presenting on MHC class-II, active
551 and resting macrophages.

552 **Fig 15.** (a) Epithelial cells. Total count broken down to active, antigen-infected and presenting on
553 class-I MHC molecule. (b) Cytokines. Concentration of cytokines and interleukins. D in the inset
554 plot is danger signal together with leukocyte growth factor IL-2.

555 3.13. Codon adaptation and *in-silico* plasmid cloning

556 The length of the optimized vaccine codon sequence was 1,386 nucleotides. The original GC-
557 Content submitted protein was 40.892862223204. The GC content of the improved sequence on
558 the Java codon optimization tool (JCAT) became 70.77922077922078 % which is highly effective
559 for translational efficiency. The calculated codon adaptive index was 0.955790963248539. The
560 NEBcutter Verstion 3.0.17 server software (https://nc3.neb.com/NEBcutter/) was used to map out
561 the restriction enzymes on the JCAT codon optimized sequence of the MEV construct. The DNA
562 sequence coding proteins for the MEV was inserted between HindIII and BamHI in the multiple
563 cloning site (MCS). In-silico cloning was done using the SnapGene software. The estimated length
564 of the Plasmid-MEV clone was 6844 bp (Fig. 16).

565 **Fig 16. In-silico cloning of the final MEV in pcDNA3.1_CT-GFP expression vector.** The red
566 part indicate the coding gene for the multi-epitope vaccine. The black part indicates the plasmid
567 vector backbone. The pDNA size is 6844 bp.

568 4. Discussion

569 OMPs roles in antibiotic resistance, as control centers of the cell for access of exogenous
570 information, and potential applications as biosensors makes them advantageous as vaccine
571 candidates. The design of computational chimeric membrane proteins seeks to harness the power
572 of these gateways and signaling networks expressed by OMPs [62]. This study combined the
573 immunogenicity of OMPs and *fliC* in the design of a novel MEV.

574 A total of 29 epitopes were predicted to be capable of eliciting both cellular and humoral immune
575 responses via the activation of T-cell and B-cell responses. 15 CTL epitopes were predicted across
576 the three classes of OMPs using stipulated thresholds in this study. Epitope "IEYAITPEI" was
577 found to be replicated in OmpA MHC class I and MHC class II epitopes and also in OmpC MHC

578 I epitopes. All epitopes were highly conserved at with a minimum and maximum conservancy
579 identity at 100 % (Table 4), ensuring the vaccine is efficacious against the diverse bacterial
580 variants. All the CTL peptide epitopes also showed highly exposed residue, therefore capable of
581 triggering an adequate cytotoxic response. Generally CD8+ T-cell recognizes the antigen of a
582 pathogen after its attachment with the MHC I molecules, therefore triggering a cytotoxic response
583 against the pathogen [63]. All selected epitopes were non-toxic and non-allergic therefore
584 decreasing the tendency for our vaccine candidates eliciting a type II hypersensitivity reaction and
585 cellular apoptosis via toxigenic reactions. Eight (8) HTL epitopes were also predicted across the
586 three classes of OMPs using stipulated thresholds and immunogenicity scores. They were further
587 subjected to IFN-γ induction capacity, as the release of IFN-γ by the CD4+ helper T-cell population
588 contributes to necessary effector cell activation and the generation of antibody mediated responses
589 to infections [64]. IFN-γ has a critical role in recognizing and eliminating pathogens. It is a central
590 effector of cell mediated immunity and also coordinates a plethora of anti-microbial functions and
591 critical in mediating intestinal immunity to *Salmonella* spp. [64, 65]. The findings of this study
592 predicted that two HTL epitopes, "LAPDRRVEI" and "IEYAITPEI" could induce IFN-γ
593 production (Table 6). This finding is satisfactory as IFN-γ is basically expected to initiate a
594 signaling cascades of receptor-ligand interactions (i.e. other cytokines and pattern recognition
595 receptors (PRRs) such as interleukin-4 (IL-4), TNF-α, and lipopolysaccharides [64, 66]. More so,
596 over-activity of IFN-γ has been reported to cause excessive tissue damage, necrosis and
597 inflammation and may contribute to disease pathology [64].

598 Seven linear B-cells epitopes were predicted. Their corresponding position, length,
599 sequence and antigenicity can be seen in Table 5. These Seven antigenic B-cell epitopes in this
600 study were selected based on artificial neural network (ANN), and the Kolaskar and Tongaonkar

601 antigenicity scale method of the IEDB server. The Kolaskar and Tongaonkar antigenicity scale
602 method predicts with a 75 % accuracy the antigenic determinants of a protein than other known
603 methods. The linear B-cell epitopes predicted had a non-toxic attribute and were non-allergenic
604 making them an ideal vaccine candidate. The B-cell epitope prediction results signifies that the
605 hydrophobic residues, such as cysteine, leucine, and valine, on the surface of proteins tend to have
606 antigenic characteristics [67].

607 When designing a vaccine, consideration is given to the population coverage capacities of
608 the MHC class I and MHC class II T cell epitopes predicted. The presence of over a thousand
609 human MHC allele across the world is a significant factor that must be considered, as only those
610 who possess a particular MHC allele recognizing the epitope in our vaccine construct will launch
611 an immunological response upon vaccination [68, 69]. The global population coverage of our
612 vaccine was 94.91 % which signifies that over 94 % of the world population will be conferred
613 protection if immunized with a vaccine preparation containing the listed CD8+ and CD4+ T cell
614 epitope of our protein chimera. Europe had the highest population cover at 97.52 % (Fig 1) and
615 will have a significantly higher protection from our vaccine chimera than any other region in the
616 World. *Salmonella* Kentucky *ST198* was first identified in Egypt and now widespread in Africa
617 [3, 70, 71, 72], we were particularly interested in seeing how our vaccine coverage performed with
618 respect to the different regions in Africa. The coverage of the vaccine on the African content was
619 significantly plausible at 85.14 % across all regions, the CD8+ T cell epitope had a significantly
620 higher coverage than its CD4+ T cell counterpart (Table 7). The vaccine coverage in North Africa
621 was astronomically higher than all other region standing at 92.89 % class combined average. At
622 52.24 % the CD4+ T cell coverage in North Africa was almost twice the population cover for the
623 other region by the same class of T-cell (Table 7). The variations exhibited in these regions may

624 be attributed to the ethnicity and race as seen from the dataset. There is a mixed race of Arabs,
625 Caucasoid, Black, and the Tunisia Berber having a combined similarity in alleles to Europe and
626 Africa combined than to the rest of the Black African regions when compared. In a recent study,
627 variations seen in population coverage was attributed to the IEDB server population coverage tool
628 having less deposition of alleles from continents like Africa and Asia as compared to the Europe
629 and America [59], and this may also be responsible for the variation seen in our study.

630 The MEV was constructed using the predicted T-cell epitopes, B-cell epitopes and *fliC*
631 protein and linked using AAY, GPGPG and EAAK protein linkers (Fig 2 and Fig 4). Linkers play
632 an important role in maintaining immunogenicity and properties of proteins in a MEV chimera. A
633 MEV without linkers may result in a new protein with unknown properties or may result in the
634 formation of neo-epitopes and or junctional epitopes [73, 74]. Also, from an immunological
635 standpoint, protein fusions are attractive since each antigen of the fusion takes advantage of the
636 additional T-cell help provided by the T-cell epitopes of the partner thus; resulting in an enhanced
637 antigen-specific immunogenicity and antibody titers [75]. The physicochemical properties of the
638 MEV construct revealed a highly antigenic, non-allergenic and non-toxic chimera. The molecular
639 weight was 47.343 kD with a theoretical PI of 9.150. Theoretically the molecular weight of a
640 peptide used in MEV should be less than 110 kD [76, 77], and the theoretical PI score indicates
641 that our MEV chimera is basic in nature. The MEV was predicted to be thermo stable, soluble
642 (Hydrophilic) and composed of more random coils (69.91 %) from the protein secondary structure
643 (Fig 3). The high proportion of random coils in the MEV only affirms that the protein is likely to
644 have an efficient antigenic potential [77, 78]. It could also represent the natural antigenicity of
645 native unfolded alpha- helices secondary structure [18]. The Ramachandran plot result showed
646 that the overall 3D model of the MEV is adequate as more than 95 % of residues were located in

647 the allowed region (Fig 5). ERRAT verification also corroborated the stereo-chemical accuracy of
648 the MEV 3D structure.

649 Evaluation of protein-protein interactions showed that the least energy values of all our
650 docked complex shows a stable TLR-MEV interactions (Table 9). Molecular simulation analysis
651 also indicated a less chance of deformation of the complexes during immune response activity
652 based on their maximum eigenvalues (Fig 8 to Fig 11) [54]. In order to predict the likelihood of
653 these complexes been formed, the Gibbs free energy (ΔG) was quantified. In thermodynamics
654 terms, Gibbs free energy (ΔG), or binding affinity of a complex is a quantitative analysis for the
655 determination of actual interaction in a cell at specific conditions [79]. The results of this study
656 revealed that all of the TLR-MEV docked complexes were energetically feasible, as indicated by
657 the negative values of Gibbs free energy (ΔG) and the multiple intermolecular contacts (Table 10).
658 This confirms that our MEV possess the capacity to induce, bind and sustain adequate
659 immunological interactions.

660 The C-ImmSim server was employed to predict the stimulated immune response against
661 our MEV. These simulations predictions provide results that match those observed in real-life
662 immunological response [18]. The administration and repetitive exposure of the MEV elicited
663 adequate B-cell isotypes and B-cell Memory cells. These cells were produced and sustained over
664 extensive number of days (Fig 12a). B-cell lymphocytes and its isotype functions in antibody
665 production and generation of protective immunity [80]. Adequate CD4+ Th cells and CD8+ T-
666 cells were also elicited following the administration of MEV. These T-cells classes elicited by our
667 MEV are a critical component of adaptive immunity in *Salmonella* infection, and a robust T-cell
668 response is required for both clearance of primary infection and resistance to subsequent challenge
669 (Cummings *et al*., 2009). Because *Salmonella* is known to reside within intra-macrophage

670 phagosomes, recent studies have highlighted a collaboration of CD4+ helper cells, and B-cell
671 responses in mediating resistance to *Salmonella* infection [81], as exhibited by our MEV
672 stimulations. Similarly there was a concomitant production of NK cells, dendritic cells and
673 macrophages following the first dose of the MEV. Cytokines, IFN-γ, TGF-b, IL-2, IL-10 and IL-
674 12 were significantly elicited and sustained (Fig. 15b). The overall activity of our MEV following
675 immune simulation can imply that our choice of epitopes significantly stimulated the required
676 immunological responses necessary for the protection and the clearance of *Salmonella* following
677 infection. In mammalian expression systems, the codon optimization strategy consists of
678 increasing the proportion of preferred mammalian codons in target genes. The noticeable high GC
679 content of 70.78 % of the improved MEV protein sequence and the CAI score of over 0.95 signifies
680 a likely effective expression of our target genes in humans as codon usage in human are larger than
681 most other non-mammalian species reaching more than 95 % GC3 content. Interestingly, GC-rich
682 genes are also well expressed several-fold to over a 100-fold more efficiently than GC-poor
683 counterparts [82].

684 5. Conclusion

685 Based on the results from this study, the following conclusions were drawn; the selected MHC
686 class I and MHC class II epitopes were antigenic, non-allergenic, and non-toxigenic and will
687 provide 94.91 % population coverage when used in a MEV construction. Epitopes "LAPDRRVEI"
688 and "IEYAITPEI" are IFN-γ inducing epitopes, and all epitopes selected for the MEV were 100
689 % conserved. The MEV protein construct was made up of 16.67 %, alpha-helices, 8.87 % extended
690 beta strands, 4.55 % beta turns, and 69.91 % random coils. The MEV was also Soluble,
691 thermostable, basic in nature, with a molecular weight of 47.343kd. Molecular dynamic simulation

692 of docked complexes of the MEV and TLRs indicated that the formation of these complexes were
693 energetically feasible, they possessed a high binding affinity with eigenvalues indicating a lesser
694 chance of deformation during immunological activity, and finally, the MEV induced adequate IgM
695 and IgG responses and their isotypes, CD4+ and CD8+ T-cells, NK cells, dendritic cells,
696 macrophages and cytokines including; IFN-γ, TGF-b, IL-2, IL-10 and IL-12. The result from this
697 in silico studies although commendable should be subjected to an *in-vitro*, pre-clinical and clinical
698 validation.

699 # Acknowledgements

700 The authors are thankful to the staff of Bacterial vaccine production department, National
701 Veterinary Research Institute Vom, Nigeria for their technical support during the course of this
702 research.

703 # Author Contributions

704 **Conceptualization:** Elayoni E. Igomu

705 **Data curation:** Elayoni E. Igomu, David O. Ehizibolo

706 **Investigation:** Elayoni E. Igomu, Paul H. Mamman, Jibril Adamu

707 **Methodology:** Elayoni E. Igomu, David O. Ehizibolo, Paul H. Mamman, Jibril Adamu,
708 Abubakar O. Woziri

709 **Resources:** Maryam Muhammad

710 **Software:** Elayoni E. Igomu, Abubakar O. Woziri

711 **Supervision:** David O. Ehizibolo, Paul H. Mamman, Jibril Adamu

712 **Writing – Review and editing:** Elayoni E. Igomu, John A. Benshak, David O.
713 Ehizibolo, Paul H. Mamman, Maryam Muhammad

714 References

715 1. Millan AS. Evolution of Plasmid-Mediated Antibiotic Resistance in the Clinical Context.
716 Trends Microbiol. 2018;26(12):978-985. doi: 10.1016/j.tim.2018.06.007.
717 2. Tacconelli E, Carrara E, Savoldi A, Harbarth S, Mendelson M, Monnet DL, et al. WHO
718 Pathogens Priority List Working Group. Discovery, research, and development of new
719 antibiotics: the WHO priority list of antibiotic-resistant bacteria and tuberculosis. Lancet
720 Infect Dis. 2018;18(3):318–327. doi: 10.1016/S1473-3099(17)30753-3. PMID: 29276051.
721 3. Hawkey J, le Hello S, Doublet B, Granier SA, Hendriksen RS, Fricke WF, et al. Global
722 phylogenomics of multidrug-resistant Salmonella enterica serotype Kentucky ST198.
723 Microb Genom. 2019;5:1–12.
724 4. Wołkowicz T, Zacharczuk K, Gierczyński R, Nowakowska M, Piekarska K. Antimicrobial
725 Resistance and Whole-Genome Characterisation of High-Level Ciprofloxacin-Resistant
726 Salmonella enterica Serovar Kentucky ST198 Strains Isolated from Human in Poland. Int
727 J Mol Sci. 2021;22(17):9381. doi: 10.3390/ijms22179381.
728 5. Micoli F, Bagnoli F, Rappuoli R, Serruto D. The role of vaccines in combatting
729 antimicrobial resistance. Nat Rev Microbiol. 2021;19(5):287–302. doi: 10.1038/s41579-
730 020-00506-3.

731 6. Kennedy DA, Read AF. Why the evolution of vaccine resistance is less of a concern than
732 the evolution of drug resistance. Proc Natl Acad Sci U S A. 2018;115(51):12878–12886.
733 doi: 10.1073/pnas.1717159115.
734 7. Rappuoli R, Santoni A, Mantovani A. Vaccines: An achievement of civilization, a human
735 right, our health insurance for the future. J Exp Med. 2019;216(1):7–9. doi:
736 10.1084/jem.20182160.
737 8. Bagnoli F, Payne DJ. Reaction: Alternative Modalities to Address Antibiotic-Resistant
738 Pathogens. Chem. 2017;3(3):369–372.
739 9. Confer AW, Ayalew S. The OmpA family of proteins: roles in bacterial pathogenesis and
740 immunity. Vet Microbiol. 2013;163(3-4):207–222. doi: 10.1016/j.vetmic.2012.08.019.
741 10. Saxena MK, Singh Y, Saxena A, Kumar R, Bhatt P. Immunogenic Outer membrane
742 Proteins (Omps) of Salmonella: Potential Candidate for sub-unit vaccine. Virol Immunol
743 J. 2017;1(2):000109.
744 11. Maiti B, Dubey S, Munang'andu HM, Karunasagar I, Karunasagar I, Evensen O.
745 Application of Outer Membrane Protein-Based Vaccines against Major Bacterial Fish
746 Pathogens in India. Front Immunol. 2020;11:1362. doi: 10.3389/fimmu.2020.01362.
747 12. Grund ME, Soo JC, Cote CK, Berisio R, Lukomski S. Thinking outside the Bug: Targeting
748 Outer Membrane Proteins for Burkholderia Vaccines. Cells. 2021;10(3):495. doi:
749 10.3390/cells10030495.
750 13. Pereira VB, Zurita-Turk M, Saraiva TDL, De Castro CP, Souza BM, Agresti PM, et al.
751 DNA vaccines approach: From concepts to applications. World J Vaccines. 2014;4(2):50–
752 71.

753 14. Schager AE, Dominguez-Medina CC, Necchi F, Micoli F, Goh YS, Goodall M, et al. IgG
754 responses to porins and lipopolysaccharide within an outer membrane-based vaccine
755 against nontyphoidal Salmonella develop at discordant rates. mBio. 2018;9(2):e02379-17.
756 doi: 10.1128/mBio.02379-17.
757 15. World Health Organization (WHO). Global Action Plan on Antimicrobial Resistance.
758 2015. Available from: http://www.who.int/drugresistance/global_action_plan/en/
759 16. Igomu EE. Salmonella Kentucky: Prevalence and challenges in Nigeria and the Africa
760 continent. Afr J Clin Exp Microbiol. 2020;21(4):272–283.
761 17. Saraiva MMS, Benevides VP, da Silva NMV, Varani AM, de Freitas Neto OC, Berchieri
762 Â Jr, et al. Genomic and Evolutionary Analysis of Salmonella enterica Serovar Kentucky
763 Sequence Type 198 Isolated from Livestock in East Africa. Front Cell Infect Microbiol.
764 2022;12:772829. doi: 10.3389/fcimb.2022.772829.
765 18. Khan Z, Ualiyeva D, Amissah OB, Sapkota S, Hameed HMA, Zhang T. Insight Into Novel
766 Anti-tuberculosis Vaccines by Using Immunoinformatics Approaches. Front Microbiol.
767 2022;13:866873. doi: 10.3389/fmicb.2022.866873.
768 19. Beikzadeh B. Immunoinformatics design of multi-epitope vaccine using OmpA, OmpD
769 and enterotoxin against non-typhoidal salmonellosis. BMC Bioinformatics. 2023;24(1):63.
770 doi: 10.1186/s12859-023-05183-6.
771 20. Procter JB, Carstairs GM, Soares B, Mourão K, Ofoegbu TC, Barton D, et al. Alignment
772 of Biological Sequences with Jalview. Methods Mol Biol. 2021;2231:203–224. doi:
773 10.1007/978-1-0716-1036-7_13.

774 21. Zafar S, Ajab H, Mughal ZU, Ahmed Zai J, Baig S, Baig A, et al. Prediction and evaluation
775 of multi epitope based sub-unit vaccine against Salmonella Typhimurium. Saudi J Biol Sci.
776 2022;29(2):1092–1099. doi: 10.1016/j.sjbs.2021.09.061.
777 22. Jensen KK, Andreatta M, Marcatili P, Buus S, Greenbaum JA, Yan Z, Sette A, et al.
778 Improved methods for predicting peptide binding affinity to MHC class II molecules.
779 Immunology. 2018;154(3):394–406. doi: 10.1111/imm.12889.
780 23. Dey J, Mahapatra SR, Patnaik S, Lata S, Kushwaha GS, Panda RK, et al. Molecular
781 Characterization and Designing of a Novel Multiepitope Vaccine Construct against
782 Pseudomonas aeruginosa. Int J Pept Res Ther. 2022;28(2):49. doi: 10.1007/s10989-021-
783 10356-z.
784 24. Nielsen M, Lundegaard C, Lund O. Prediction of MHC class II binding affinity using
785 SMM-align, a novel stabilization matrix alignment method. BMC Bioinformatics.
786 2007;8:238.
787 25. Doytchinova IA, Flower DR. VaxiJen: a server for prediction of protective antigens,
788 tumour antigens and subunit vaccines. BMC Bioinformatics. 2007;8:4. doi: 10.1186/1471-
789 2105-8-4.
790 26. Chatterjee R, Sahoo P, Mahapatra SR, Dey J, Ghosh M, Kushwaha GS, et al. Development
791 of a Conserved Chimeric Vaccine for Induction of Strong Immune Response against
792 Staphylococcus aureus Using Immunoinformatics Approaches. Vaccines. 2021;9(9):1038.
793 doi: 10.3390/vaccines9091038.
794 27. Dey J, Mahapatra SR, Raj TK, Kaur T, Jain P, Tiwari A, et al. Designing a novel multi-
795 epitope vaccine to evoke a robust immune response against pathogenic multidrug-resistant

796 Enterococcus faecium bacterium. Gut Pathog. 2022;14(1):21. doi: 10.1186/s13099-022-
797 00495-z.
798 28. Ali MC, Khatun MS, Jahan SI, Das R, Munni YA, Rahman MM, Dash R. In-silico design
799 of epitope-based peptide vaccine against non-typhoidal Salmonella through
800 immunoinformatic approaches. J Biomol Struct Dyn. 2021;40(21):10696-10714.
801 29. Mahapatra SR, Dey J, Jaiswal A, Roy R, Misra N, Suar M. Immunoinformatics-guided
802 designing of epitope-based subunit vaccine from Pilus assembly protein of Acinetobacter
803 baumannii bacteria. J Immunol Methods. 2022;508:113325. doi:
804 10.1016/j.jim.2022.113325.
805 30. Moodley A, Fatoba A, Okpeku M, Emmanuel Chiliza T, Blessing Cedric Simelane M,
806 Pooe OJ. Reverse vaccinology approach to design a multi-epitope vaccine construct based
807 on the Mycobacterium tuberculosis biomarker PE_PGRS17. Immunol Res.
808 2022;70(4):501–517. doi: 10.1007/s12026-022-09284-x.
809 31. Dhanda SK, Vir P, Raghava GPS. Designing of interferon-gamma inducing MHC class-II
810 binders. Biol Direct. 2013;8(1):30. doi: 10.1186/1745-6150-8-30.
811 32. Sanches RCO, Tiwari S, Ferreira LCG, Oliveira FM, Lopes MD, Passos MJF, et al.
812 Immunoinformatics Design of Multi-Epitope_Peptide-Based Vaccine against Schistosoma
813 mansoni Using Transmembrane Proteins as a Target. Front Immunol. 2021;12:621706.
814 doi: 10.3389/fimmu.2021.621706.
815 33. Zaib S, Akram F, Liaqat ST, Altaf MZ, Khan I, Dera AA, et al. Bioinformatics approach
816 for the construction of multiple epitope vaccine against omicron variant of SARS-CoV-2.
817 Sci Rep. 2022;12(1):19087. doi: 10.1038/s41598-022-23550-w.

818 34. Bibi S, Ullah I, Zhu B, Adnan M, Liaqat R, Kong WB, Niu S. In-silico analysis of epitope-
819 based vaccine candidate against tuberculosis using reverse vaccinology. Sci Rep.
820 2021;11(1):1249. doi: 10.1038/s41598-020-80899-6.
821 35. Atapour A, Vosough P, Jafari S, Sarab GA. A multi-epitope vaccine designed against
822 blood-stage of malaria: an immunoinformatic and structural approach. Sci Rep.
823 2022;12(1):11683. doi: 10.1038/s41598-022-15956-3.
824 36. Hennebert E, Maldonado B, Ladurner P, Flammang P, Santos R. Experimental strategies
825 for the identification and characterization of adhesive proteins in animals: a review.
826 Interface Focus. 2015;5(1):20140064. doi: 10.1098/rsfs.2014.0064.
827 37. Roy Chowdhury A, Sah S, Varshney U, Chakravortty D. Salmonella Typhimurium outer
828 membrane protein A (OmpA) renders protection from nitrosative stress of macrophages by
829 maintaining the stability of bacterial outer membrane. PLoS Pathog. 2022;18(8):e1010708.
830 doi: 10.1371/journal.ppat.1010708.
831 38. Hebditch M, Carballo-Amador MA, Charonis S, Curtis R, Warwicker J. Protein-Sol: a web
832 tool for predicting protein solubility from sequence. Bioinformatics (Oxford, England).
833 2017;33(19):3098–3100. doi: 10.1093/bioinformatics/btx345.
834 39. McGuffin LJ, Bryson K, Jones DT. The PSIPRED protein structure prediction server.
835 Bioinformatics (Oxford, England). 2000;16(4):404–405. doi:
836 10.1093/bioinformatics/16.4.404.
837 40. Geourjon C, Deléage G. SOPMA: significant improvements in protein secondary structure
838 prediction by consensus prediction from multiple alignments. Comput Appl Biosci:
839 CABIOS. 1995;11(6):681–684. doi: 10.1093/bioinformatics/11.6.681.

840 41. Yang J, Yan R, Roy A, Xu D, Poisson J, Zhang Y. The I-TASSER Suite: protein structure
841 and function prediction. Nat Methods. 2015;12(1):7–8. doi: 10.1038/nmeth.3213.
842 42. Khatoon N, Pandey RK, Prajapati VK. Exploring Leishmania secretory proteins to design
843 B and T cell multi-epitope subunit vaccine using immunoinformatics approach. Sci Rep.
844 2017;7(1):8285. doi: 10.1038/s41598-017-08842-w.
845 43. Heo L, Park H, Seok C. GalaxyRefine: Protein structure refinement driven by side-chain
846 repacking. Nucleic Acids Res. 2013;41:384–388. doi: 10.1093/nar/gkt458.
847 44. Priyadarsini S, Panda S, Pashupathi M, Kumar A, Singh R. Design of Multiepitope Vaccine
848 Construct against Non-typhoidal Salmonellosis and its Characterization Using
849 Immunoinformatics Approach. Int J Pept Res Ther. 2021;27:2333–2348.
850 45. Naveed M, Ali U, Karobari MI, Ahmed N, Mohamed RN, Abullais SS, et al. A Vaccine
851 Construction against COVID-19-Associated Mucormycosis Contrived with
852 Immunoinformatics-Based Scavenging of Potential Mucoralean Epitopes. Vaccines.
853 2022;10(5):664. doi: 10.3390/vaccines10050664.
854 46. Laskowski RA, MacArthur MW, Moss DS, Thornton JM. PROCHECK: a program to
855 check the stereochemical quality of protein structures. J Appl Crystallogr. 1993;26:283-
856 291. doi: 10.1107/S0021889892009944.
857 47. Lovell SC, Davis IW, Arendall WB 3rd, de Bakker PI, Word JM, Prisant MG, Richardson
858 JS, Richardson DC. Structure validation by Calpha geometry: phi, psi and Cbeta deviation.
859 Proteins. 2003;50(3):437–450. doi: 10.1002/prot.10286.
860 48. Ponomarenko J, Bui H-H, Li W, Fusseder N, Bourne PE, Sette A, Peters B. ElliPro: a new
861 structure-based tool for the prediction of antibody epitopes. BMC Bioinformatics.
862 2008;9(1):514. doi: 10.1186/1471-2105-9-514.

863 49. Arpaia N, Godec J, Lau L, Sivick KE, McLaughlin LM, Jones MB, Dracheva T, Peterson
864 SN, Monack DM, Barton GM. TLR signaling is required for Salmonella Typhimurium
865 virulence. Cell. 2011;144(5):675–688. doi: 10.1016/j.cell.2011.01.031.
866 50. Su L, Wang Y, Wang J, Mifune Y, Morin MD, Jones BT, et al. Structural Basis of
867 TLR2/TLR1 Activation by the Synthetic Agonist Diprovocim. J Med Chem.
868 2019;62(6):2938–2949. doi: 10.1021/acs.jmedchem.8b01583.
869 51. Banerjee S, Majumder K, Gutierrez GJ, Gupta D, Mittal B. Immuno-informatics approach
870 for multi-epitope vaccine designing against SARS-CoV-2. BioRxiv: the preprint server for
871 biology. 2020.07.23.218529. doi: 10.1101/2020.07.23.218529.
872 52. Kozakov D, Hall DR, Xia B, Porter KA, Padhorny D, Yueh C, et al. The ClusPro web
873 server for protein-protein docking. Nat Protoc. 2017;12(2):255–278. doi:
874 10.1038/nprot.2016.169.
875 53. Desta IT, Porter KA, Xia B, Kozakov D, Vajda S. Performance and its limits in rigid body
876 protein-protein docking. Structure. 2020;28(9):1071-1081. doi: 10.1016/j.str.2020.06.006.
877 54. López-Blanco JR, Aliaga JI, Quintana-Ortí ES, Chacón P. iMODS: internal coordinates
878 normal mode analysis server. Nucleic Acids Res. 2014;42(Web Server issue):W271–
879 W276. doi: 10.1093/nar/gku339.
880 55. Vangone A, Bonvin AM. Contacts-based prediction of binding affinity in protein-protein
881 complexes. eLife. 2015;4:e07454. doi: 10.7554/eLife.07454.
882 56. Xue LC, Rodrigues JP, Kastritis PL, Bonvin AM, Vangone A. PRODIGY: a web server
883 for predicting the binding affinity of protein-protein complexes. Bioinformatics.
884 2016;32(23):3676–3678. doi: 10.1093/bioinformatics/btw514.

885 57. Kar T, Narsaria U, Basak S, Deb D, Castiglione F, Mueller DM, et al. A candidate multi-
886 epitope vaccine against SARS-CoV-2. Sci Rep. 2020;10(1):10895. doi: 10.1038/s41598-
887 020-67749-1.
888 58. Castiglione F, Deb D, Srivastava AP, Liò P, Liso A. From infection to immunity:
889 understanding the response to SARS-CoV2 through in-silico modeling. Front Immunol.
890 2021;12:646972.
891 59. Chukwudozie OS, Gray CM, Fagbayi TA, Chukwuanukwu RC, Oyebanji VO, Bankole
892 TT, et al. Immuno-informatics design of a multimeric epitope peptide based vaccine
893 targeting SARS-CoV-2 spike glycoprotein. PLoS One. 2021;16(3):e0248061. doi:
894 10.1371/journal.pone.0248061.
895 60. Pandey RK, Ojha R, Aathmanathan VS, Krishnan M, Prajapati VK. Immunoinformatics
896 approaches to design a novel multi-epitope subunit vaccine against HIV infection. Vaccine.
897 2018;36(17):2262–2272. doi: 10.1016/j.vaccine.2018.03.042.
898 61. Hasan M, Ghosh PP, Azim KF, Mukta S, Abir RA, Nahar J, et al. Reverse vaccinology
899 approach to design a novel multi-epitope subunit vaccine against avian influenza A (H7N9)
900 virus. Microb Pathog. 2019;130:19–37. doi: 10.1016/j.micpath.2019.02.023.
901 62. Slusky JS. Outer membrane protein design. Curr Opin Struct Biol. 2017;45:45–52. doi:
902 10.1016/j.sbi.2016.11.003.
903 63. Sigal LJ. Activation of CD8 T lymphocytes during viral infections. Encycl Immunobiol.
904 2016:286–290. doi: 10.1016/B978-0-12-374279-7.14009-3.
905 64. Kak G, Raza M, Tiwari BK. Interferon-gamma (IFN-γ): exploring its implications in
906 infectious diseases. Biomol Concepts. 2018;9(1):64–79. doi: 10.1515/bmc-2018-0007.

907 65. Bao S, Beagley KW, France MP, Shen J, Husband AJ. Interferon gamma plays a critical
908 role in intestinal immunity against Salmonella Typhimurium infection. Immunology.
909 2000;99:464-472. doi:10.1046/j.1365-2567.2000.00955.x
910 66. Gordon MA, Jack DL, Dockrell DH, Lee ME, Read RC. Gamma interferon enhances
911 internalization and early non-oxidative killing of Salmonella enterica serovar
912 Typhimurium by human macrophages and modifies cytokine responses. Infect Immun.
913 2005;73(6):3445–3452. doi:10.1128/IAI.73.6.3445-3452.2005
914 67. Yurina V, Adianingsih OR. Predicting epitopes for vaccine development using
915 bioinformatics tools. Ther Adv Vaccines Immunother. 2022;10:25151355221100218.
916 doi:10.1177/25151355221100218
917 68. Bui HH, Sidney J, Dinh K, Southwood S, Newman MJ, Sette A. Predicting population
918 coverage of T-cell epitope-based diagnostics and vaccines. BMC Bioinformatics.
919 2006;7:153. doi:10.1186/1471-2105-7-153
920 69. Ahammad I, Lira SS. Designing a novel mRNA vaccine against SARS-CoV-2: An
921 immunoinformatics approach. Int J Biol Macromol. 2020;162:820–837.
922 doi:10.1016/j.ijbiomac.2020.06.213
923 70. Le Hello S, Hendriksen RS, Doublet B, Fisher I, Nielsen EM, Whichard JM, Bouchrif B,
924 Fashae K, Granier SA, Silva NJ, Cloeckaert A, Threlfall EJ, Angulo FJ, Aarestrup FM,
925 Wain J, Weill FX. International Spread of an Epidemic Population of Salmonella enterica
926 Serotype Kentucky ST198 Resistant to Ciprofloxacin. J Infect Dis. 2011;204:675-684.
927 71. Abd-Elghany SM, Sallam KI, Abd-Elkhalek A, Tamura T. Occurrence, genetic
928 characterization and antimicrobial resistance of Salmonella isolated from chicken meat and
929 giblets. Epidemiol Infect. 2015;143(5):997–1003. doi:10.1017/S0950268814001708.

930 72. Haley BJ, Kim SW, Haendiges J, Keller E, Torpey D, Kim A, et al. Salmonella enterica
931 serovar Kentucky recovered from human clinical cases in Maryland, USA (2011-2015).
932 Zoonoses Public Health. 2019;66(4):382–392. doi:10.1111/zph.12571
933 73. Meza B, Ascencio F, Sierra-Beltrán AP, Torres J, Angulo C. A novel design of a multi-
934 antigenic, multistage and multi-epitope vaccine against Helicobacter pylori: An in silico
935 approach. Infect Genet Evol. 2017;4:309–317. doi:10.1016/j.meegid.2017.02.007
936 74. Shey RA, Ghogomu SM, Esoh KK, Nebangwa ND, Shintouo CM, Nongley NF, et al. In-
937 silico design of a multi-epitope vaccine candidate against onchocerciasis and related filarial
938 diseases. Sci Rep. 2019;9(1):4409. doi:10.1038/s41598-019-40833-x
939 75. König E, Gagliardi A, Riedmiller I, Andretta C, Tomasi M, Irene C, et al. Multi-Antigen
940 Outer Membrane Vesicle Engineering to Develop Polyvalent Vaccines: The
941 Staphylococcus aureus Case. Front Immunol. 2021;12:752168.
942 doi:10.3389/fimmu.2021.752168
943 76. Barh D, Barve N, Gupta K, Chandra S, Jain N, Tiwari S, et al. Exoproteome and secretome
944 derived broad spectrum novel drug and vaccine candidates in Vibrio cholerae targeted by
945 Piper betel derived compounds. PLoS One. 2013;8(1):e52773.
946 doi:10.1371/journal.pone.0052773
947 77. Li M, Zhu Y, Niu C, Xie X, Haimiti G, Guo W, et al. Design of a multi-epitope vaccine
948 candidate against Brucella melitensis. Sci Rep. 2022;12(1):10146. doi:10.1038/s41598-
949 022-14427-z
950 78. Yu M, Zhu Y, Li Y, Chen Z, Sha T, Li Z, et al. Design of a novel multi-epitope vaccine
951 against Echinococcus granulosus in immunoinformatics. Front Immunol. 2021;12:668492.
952 doi:10.3389/fimmu.2021.668492

953 79. Pan C. Measuring dissociation rate constants of protein complexes through subunit
954 exchange: experimental design and theoretical modeling. PLoS One. 2011;6(12):e28827.
955 doi:10.1371/journal.pone.0028827
956 80. Cummings LA, Deatherage BL, Cookson BT. Adaptive immune responses during
957 Salmonella infection. EcoSal Plus. 2009;3(2). doi:10.1128/ecosalplus.8.8.11
958 81. Griffin AJ, McSorley SJ. Development of protective immunity to Salmonella, a mucosal
959 pathogen with a systemic agenda. Mucosal Immunol. 2011;4(4):371-382.
960 doi:10.1038/mi.2011.2
961 82. Kudla G, Lipinski L, Caffin F, Helwak A, Zylicz M. High guanine and cytosine content
962 increases mRNA levels in mammalian cells. PLoS Biol. 2006;4(6):e180.
963 doi:10.1371/journal.pbio.0040180

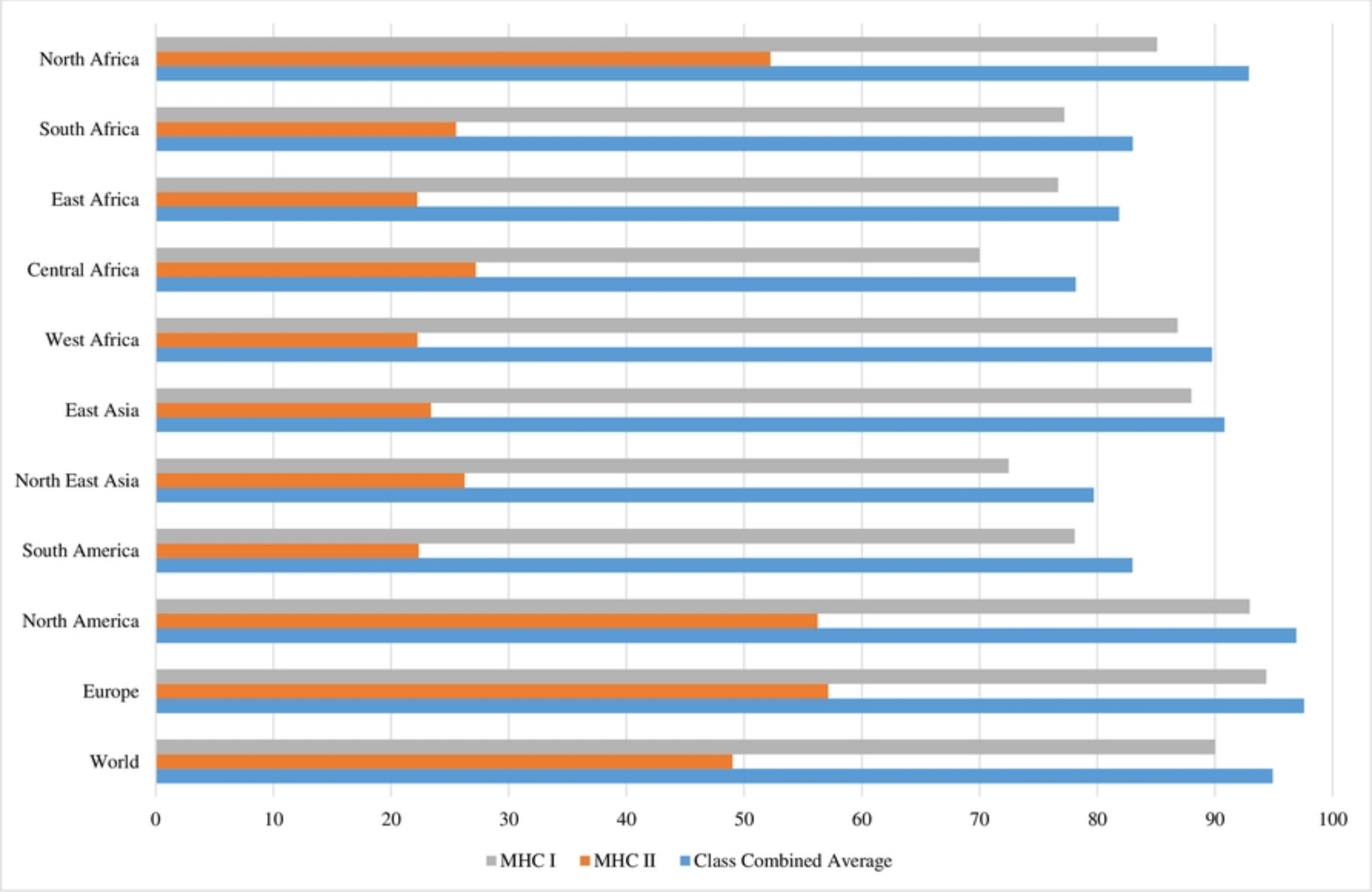
North Africa
South Africa
East Africa
Central Africa
West Africa
East Asia
North East Asia
South America
North America
Europe
World
0
10
20
30
40
50
60
70
80
90
100
MHC I
MHC II
Class Combined Average

Fig 1

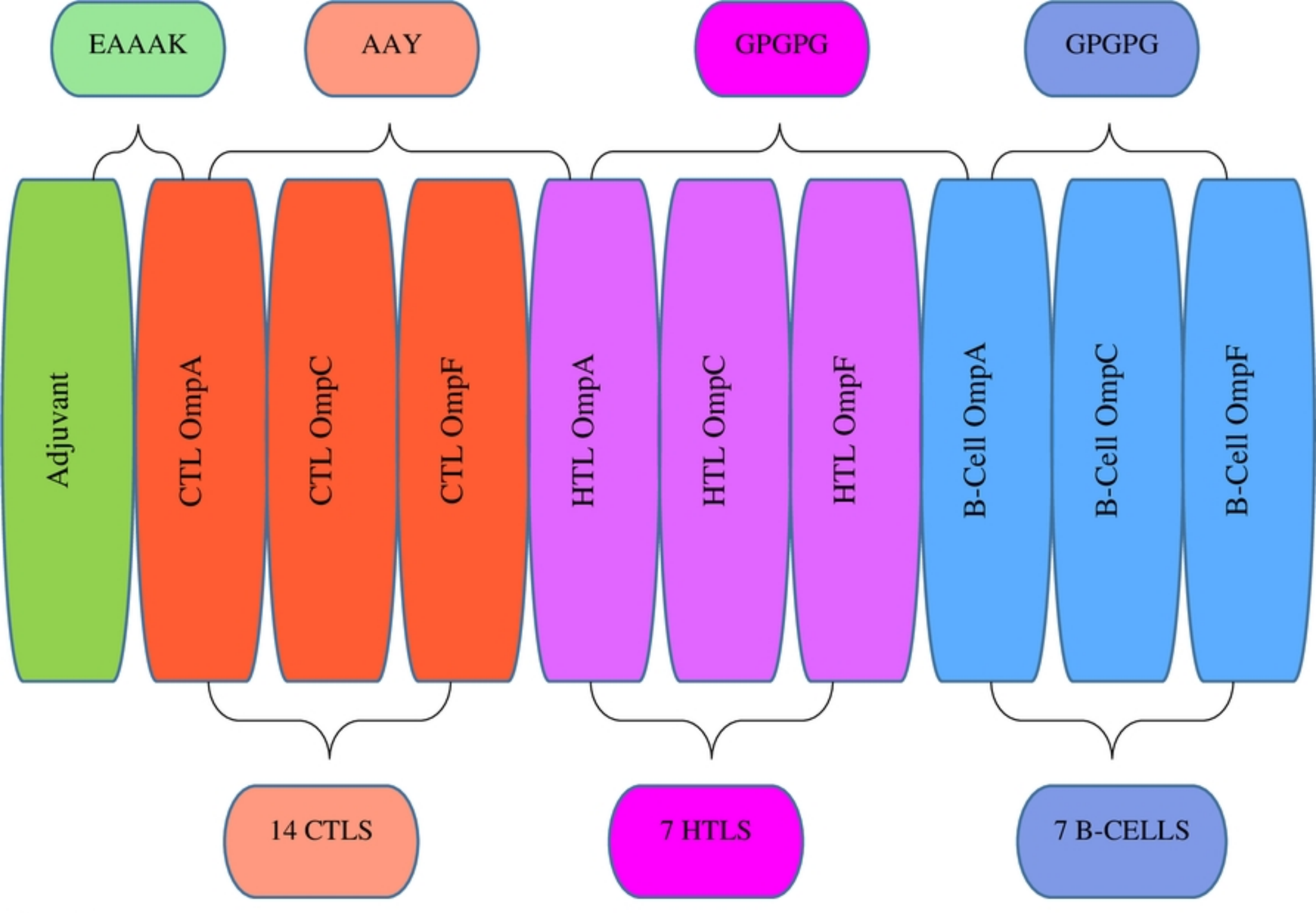
EAAAK
AAY
GPGPG
GPGPG
Adjuvant
CTL OmpA
CTL OmpC
CTL OmpF
HTL OmpA
HTL OmpC
HTL OmpF
B-Cell OmpA
B-Cell OmpC
B-Cell OmpF
14 CTLS
7 HTLS
7 B-CELLS

Fig 2

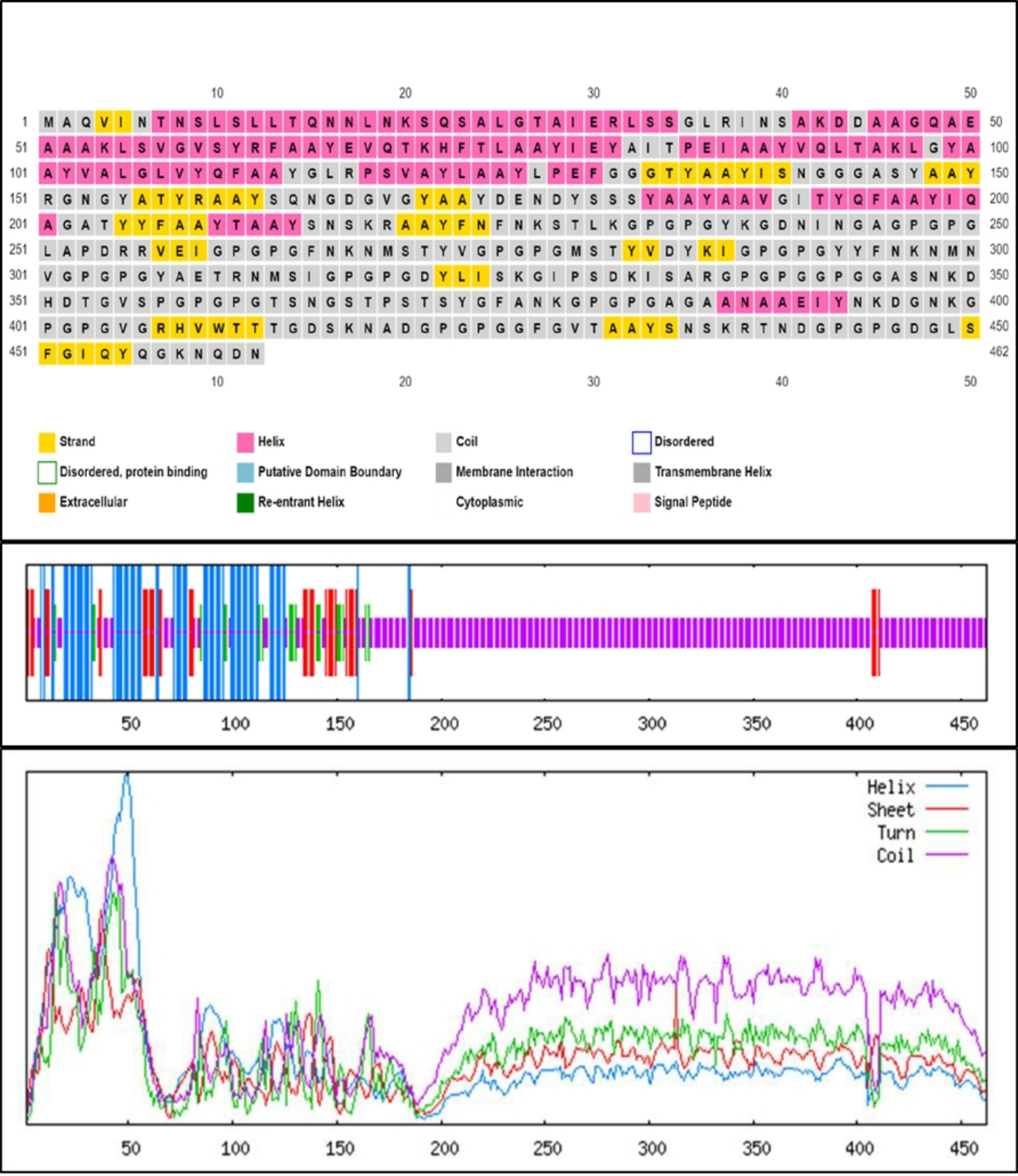
10 20 30 40 50
1 MAQVINTNSLSLLTQNNLNKSQSALGTAIERLSSGLRINSAKDDAAGQAE 50
51 AAAKLSVGVSYRFAAYEVQTKHFTLAAYIEYAITPEIAAYVQLTAKLGYA 100
101 AYVALGLVYQFAAYGLRPSVAYLAAYLPEFGGGTYAAYISNGGGASYAAY 150
151 RGNGYATYRAAYSQNGDGVGYAAYDENDYSSSYAAYAAVGITYQFAAYIQ 200
201 AGATYYFAAYTAAYSNSKRAAYFNFNKSTLKGPGPGYKGDNINGAGPGPG 250
251 LAPDRRVEIGPGPGFNKNMSTYVGPGPGMSTYVDYKIGPGPGYYFNKNMN 300
301 VGPGPGYAETRNMSIGPGPGDYLISKGIPSDKISARGPGPGGPGGASNKD 350
351 HDTGVSPGPGPGTSNGSTPSTSYGFANKGPGPGAGAANAAEIYNKDGNKG 400
401 PGPGVGRHVWTTTGDSKNADGPGPGGFGVTAAYSNSKRTNDGPGPGDGLS 450
451 FGIQYQGKNQDN 462
10 20 30 40 50
Strand
Helix
Coil
Disordered
Disordered, protein binding
Putative Domain Boundary
Membrane Interaction
Transmembrane Helix
Extracellular
Re-entrant Helix
Cytoplasmic
Signal Peptide
50 100 150 200 250 300 350 400 450
Helix
Sheet
Turn
Coil
50 100 150 200 250 300 350 400 450

Fig 3

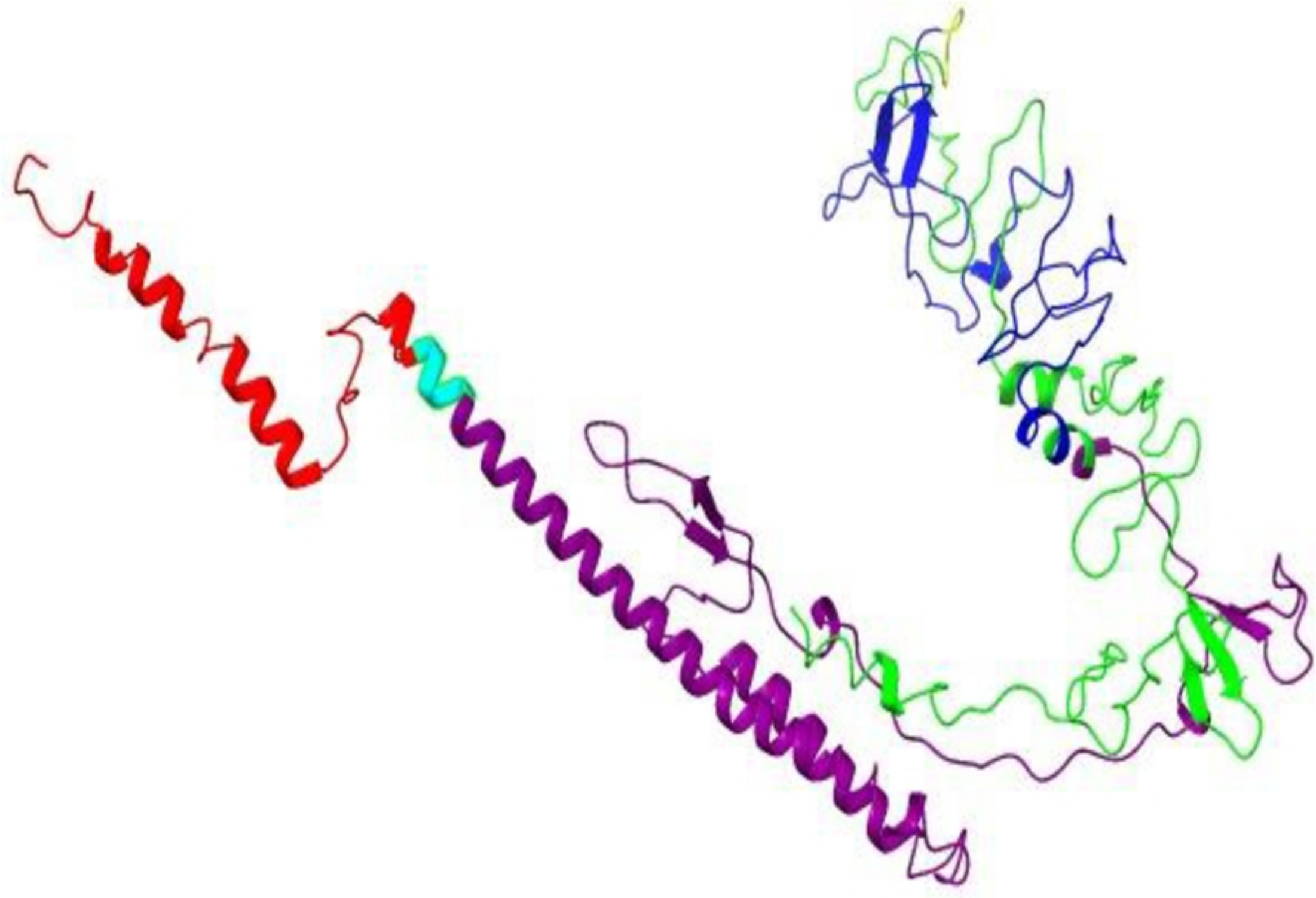

Fig 4

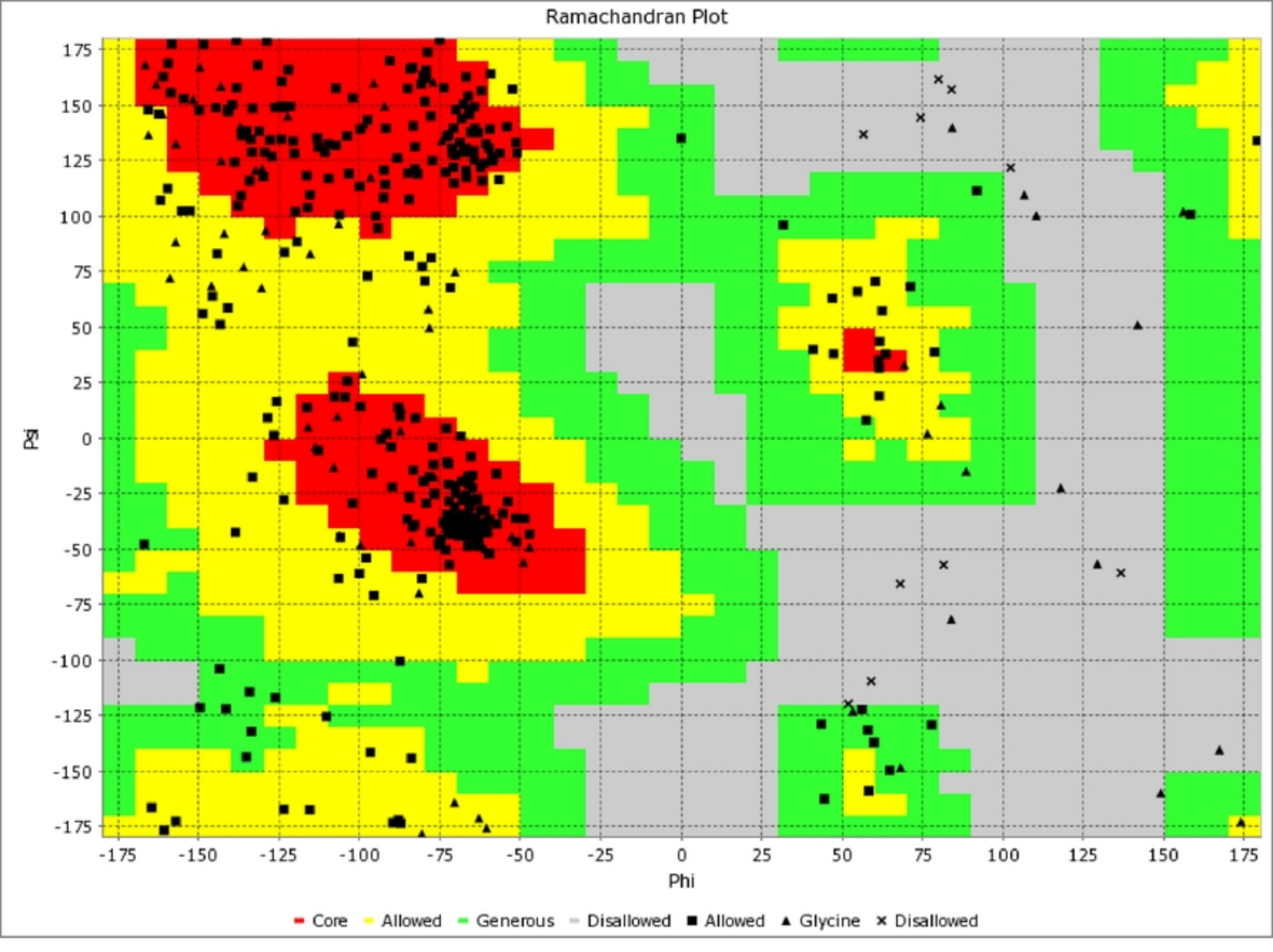
Ramachandran Plot
Psi
Phi
175
150
125
100
75
50
25
0
-25
-50
-75
-100
-125
-150
-175
Core
Allowed
Generous
Disallowed
Allowed
Glycine
Disallowed

Fig 5

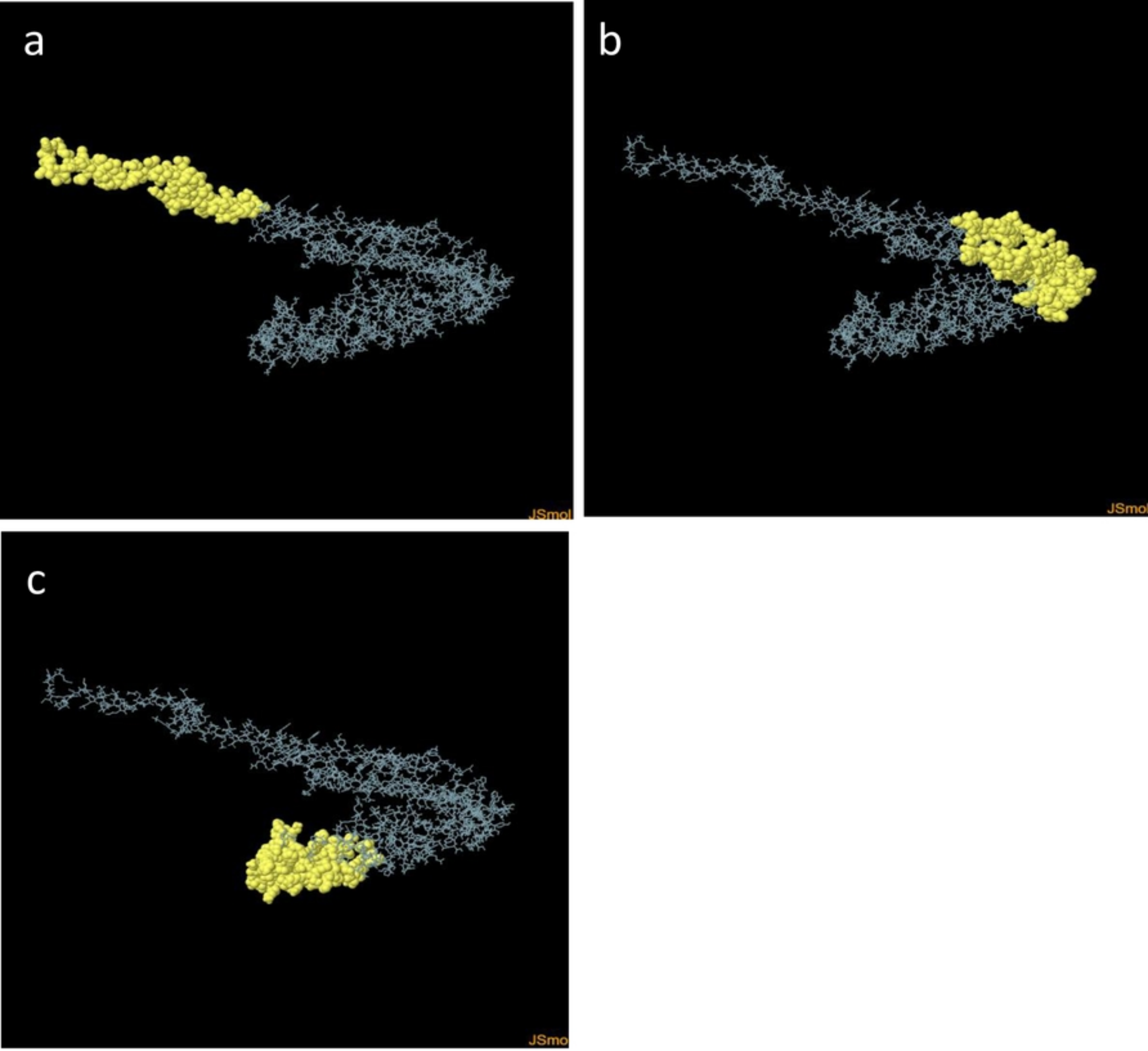

Fig 6

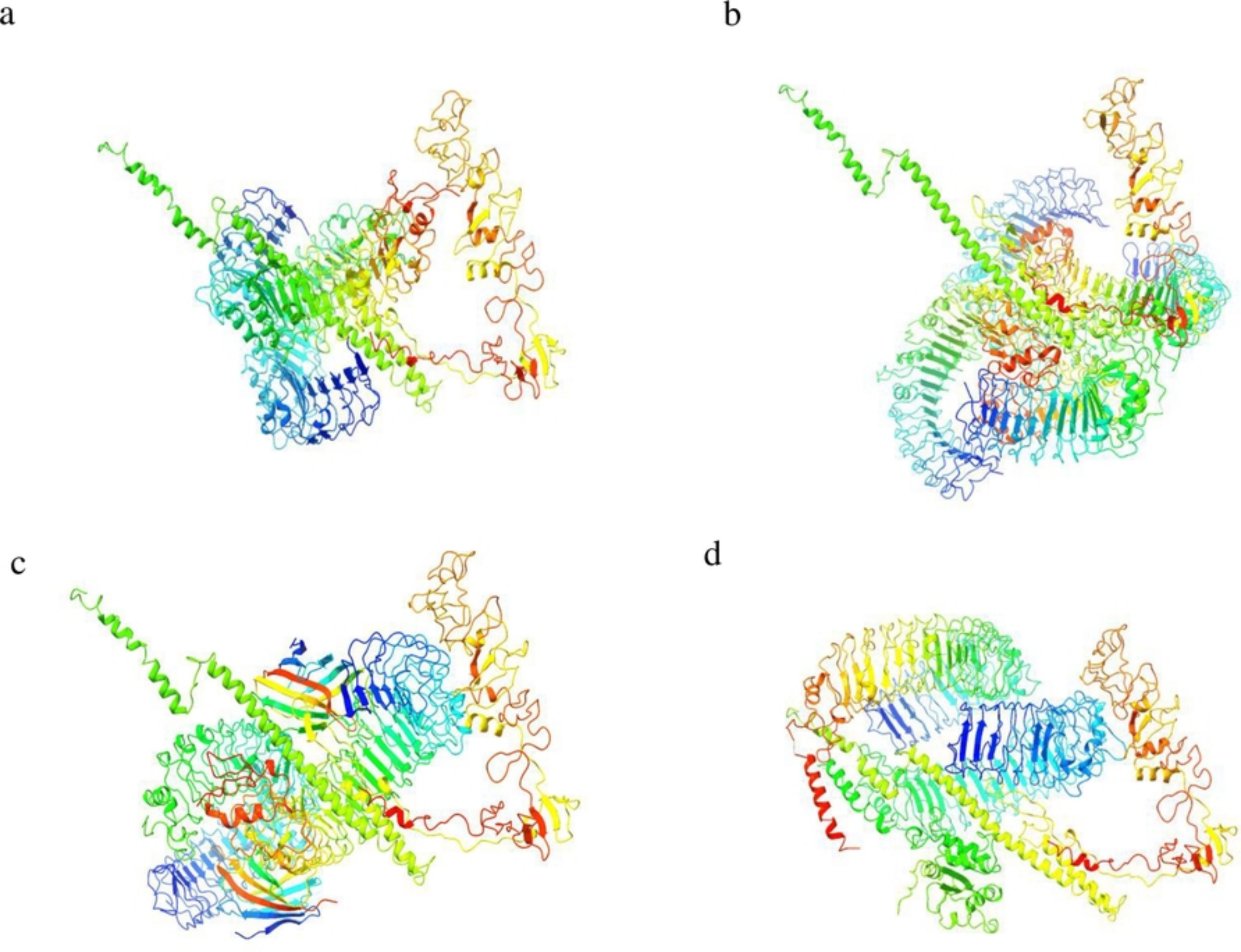

Fig 7

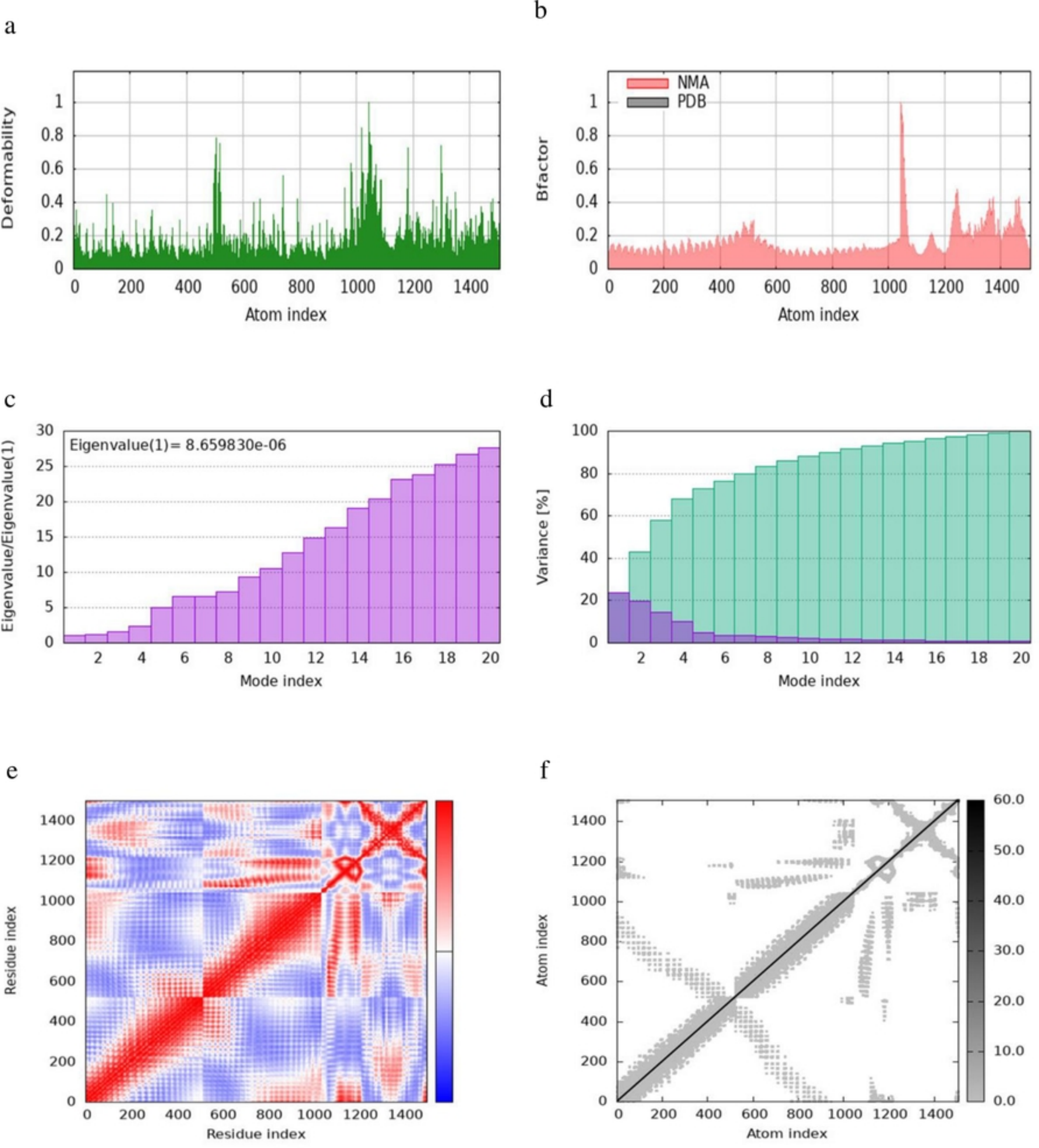
a
Deformability
Atom index
b
NMA
PDB
Bfactor
Atom index
c
Eigenvalue(1)= 8.659830e-06
Eigenvalue/Eigenvalue(1)
Mode index
d
Variance [%]
Mode index
e
Residue index
Residue index
f
Atom index
Atom index

Fig 8

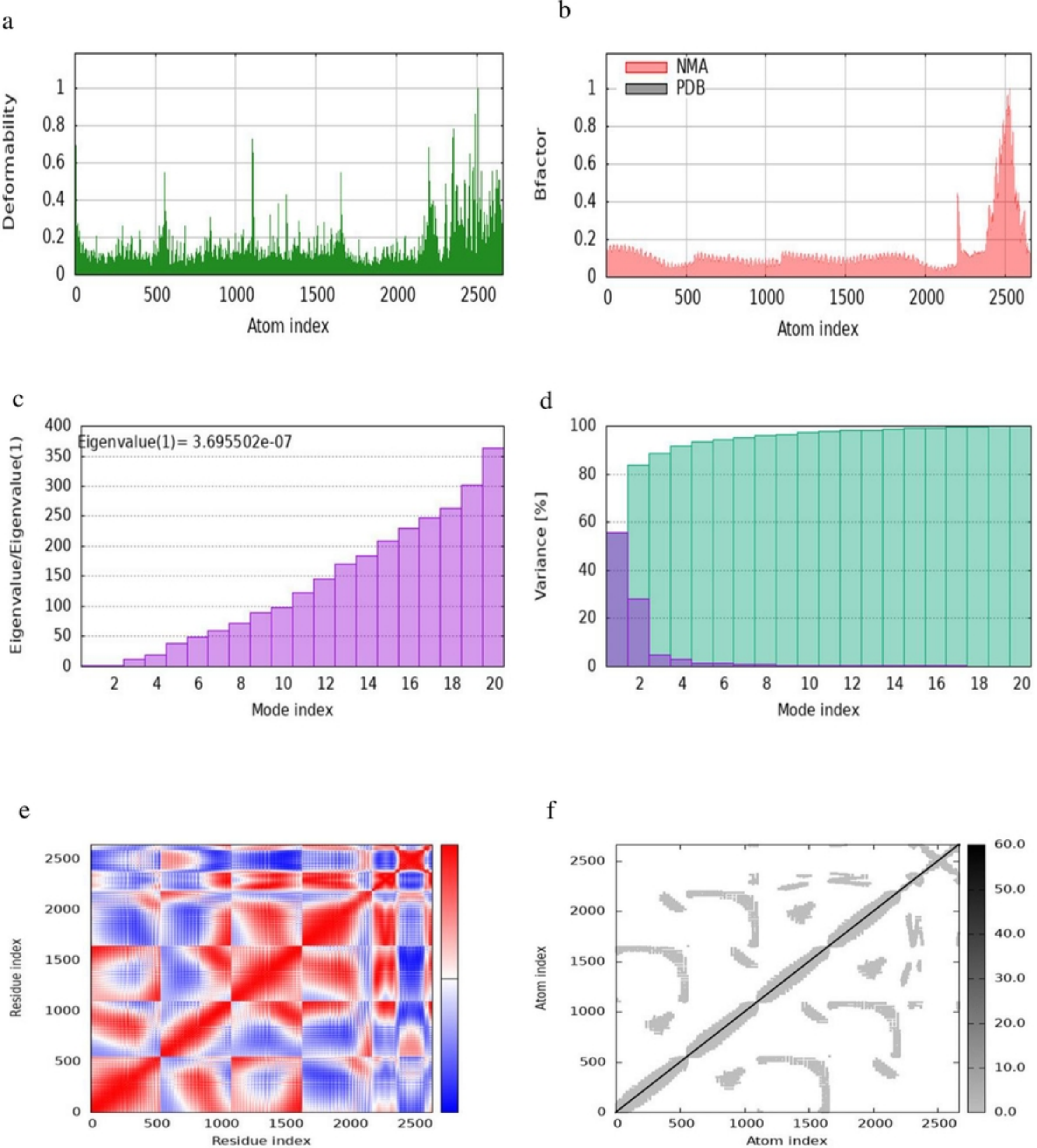
a
Deformability
Atom index
b
NMA
PDB
Bfactor
Atom index
c
Eigenvalue(1)= 3.695502e-07
Eigenvalue/Eigenvalue(1)
Mode index
d
Variance [%]
Mode index
e
Residue index
Residue index
f
Atom index
Atom index

Fig 9

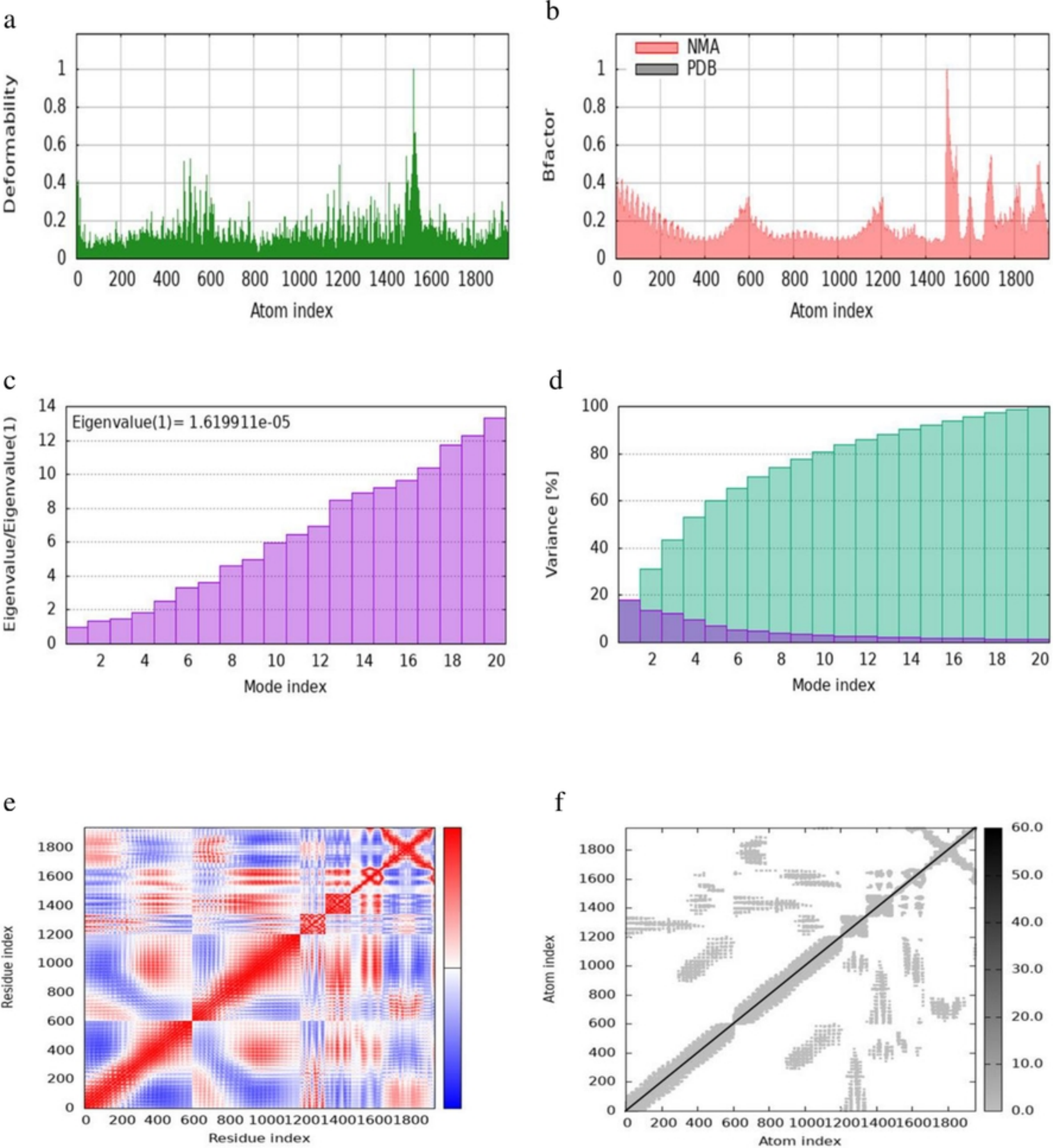
a
Deformability
Atom index
b
NMA
PDB
Bfactor
Atom index
c
Eigenvalue(1)= 1.619911e-05
Eigenvalue/Eigenvalue(1)
Mode index
d
Variance [%]
Mode index
e
Residue index
Residue index
f
Atom index
Atom index

Fig 10

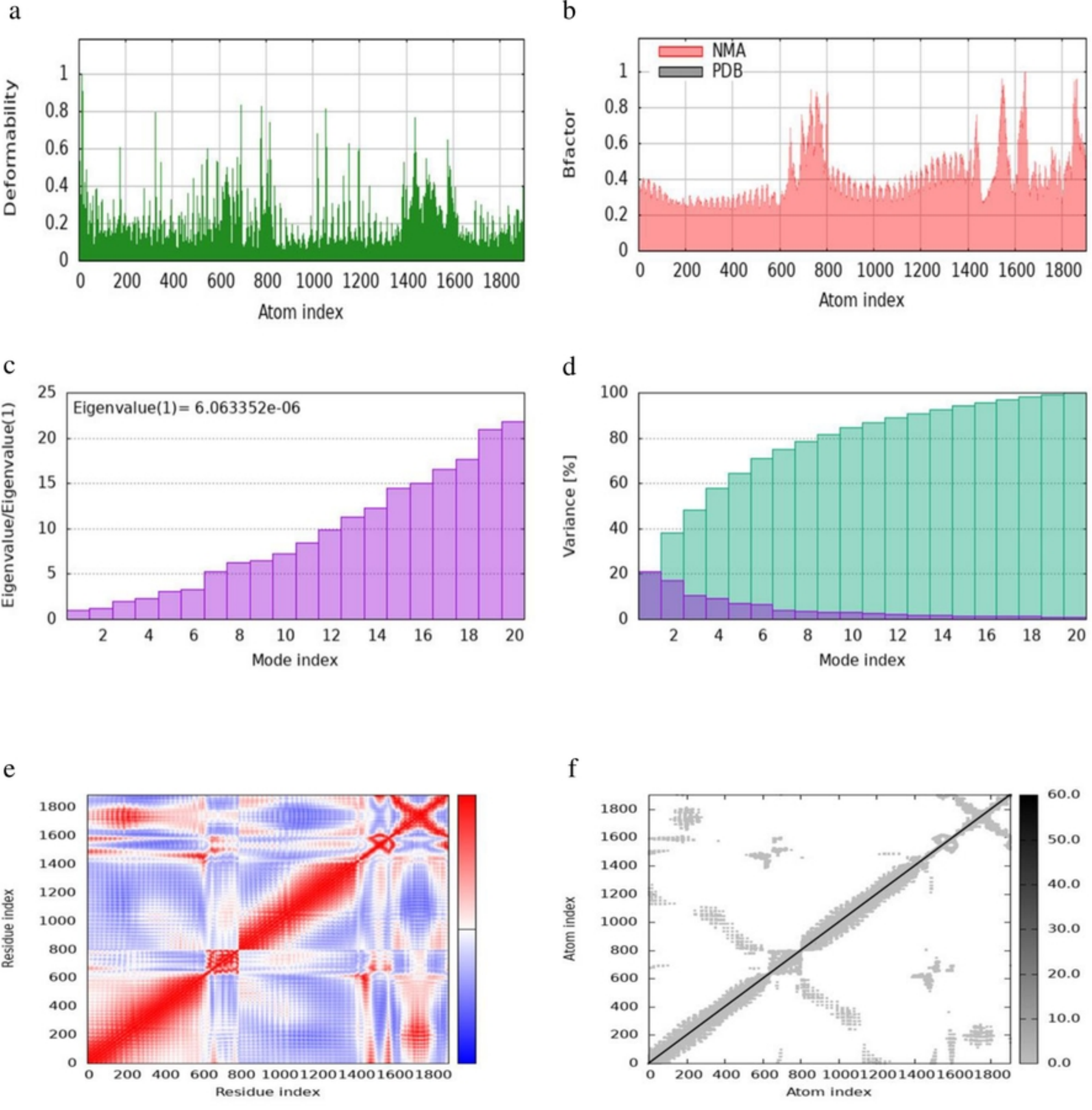
a
Deformability
Atom index
b
NMA
PDB
Bfactor
Atom index
c
Eigenvalue(1)= 6.063352e-06
Eigenvalue/Eigenvalue(1)
Mode index
d
Variance [%]
Mode index
e
Residue index
Residue index
f
Atom index
Atom index

Fig 11

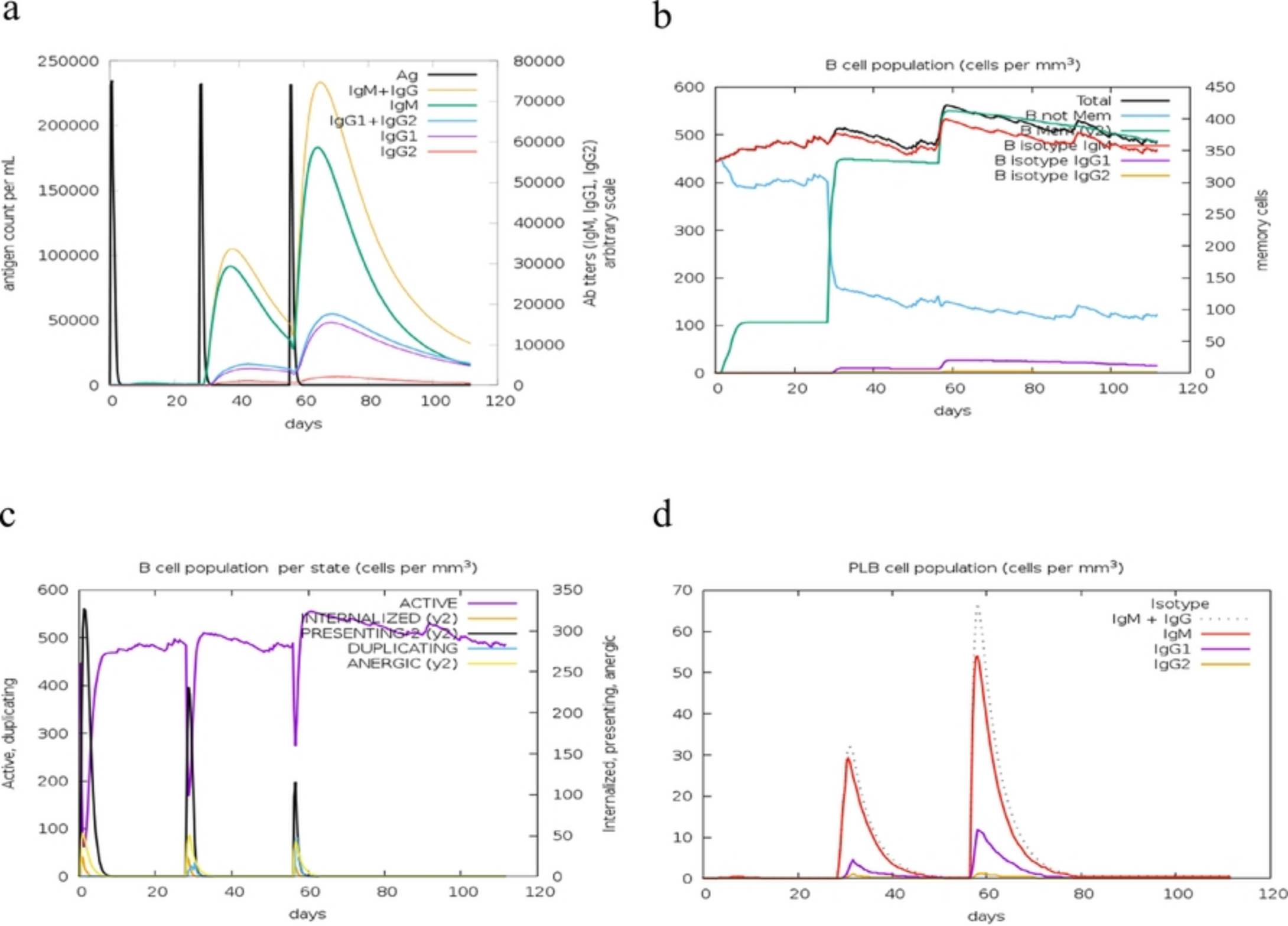
a
Ag
IgM+IgG
IgM
IgG1+IgG2
IgG1
IgG2
antigen count per mL
Ab titers (IgM, IgG1, IgG2) arbitrary scale
days
b
B cell population (cells per mm³)
Total
B not Mem
B Mem (y2)
B isotype IgM
B isotype IgG1
B isotype IgG2
memory cells
days
c
B cell population per state (cells per mm³)
ACTIVE
INTERNALIZED (y2)
PRESENTING-2 (y2)
DUPLICATING
ANERGIC (y2)
Active, duplicating
Internalized, presenting, anergic
days
d
PLB cell population (cells per mm³)
Isotype
IgM + IgG
IgM
IgG1
IgG2
days

Fig 12

a

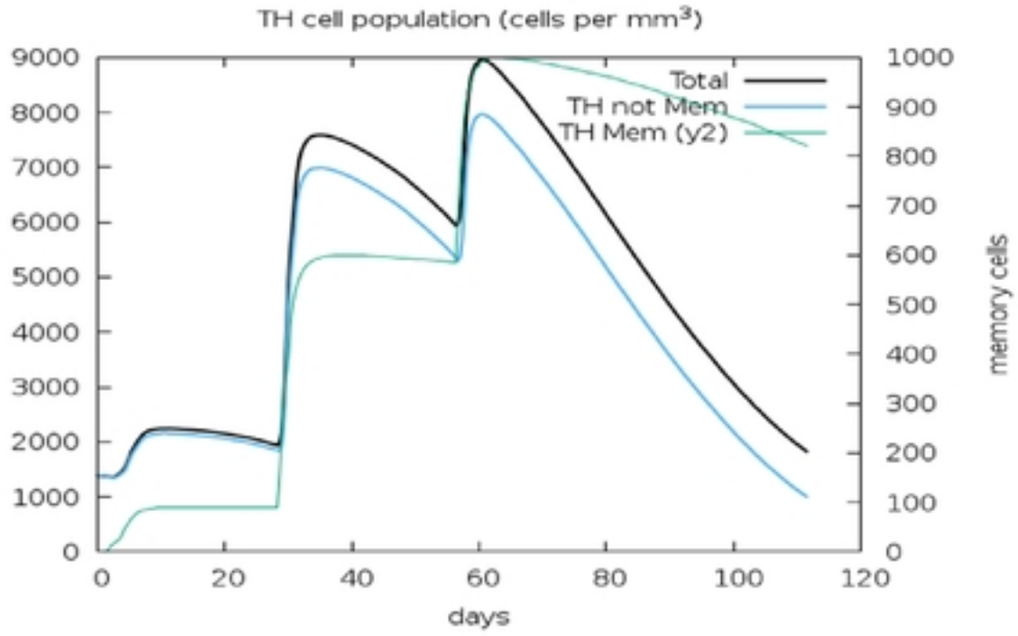
TH cell population (cells per mm³)
Total
TH not Mem
TH Mem (y2)
memory cells
days

b

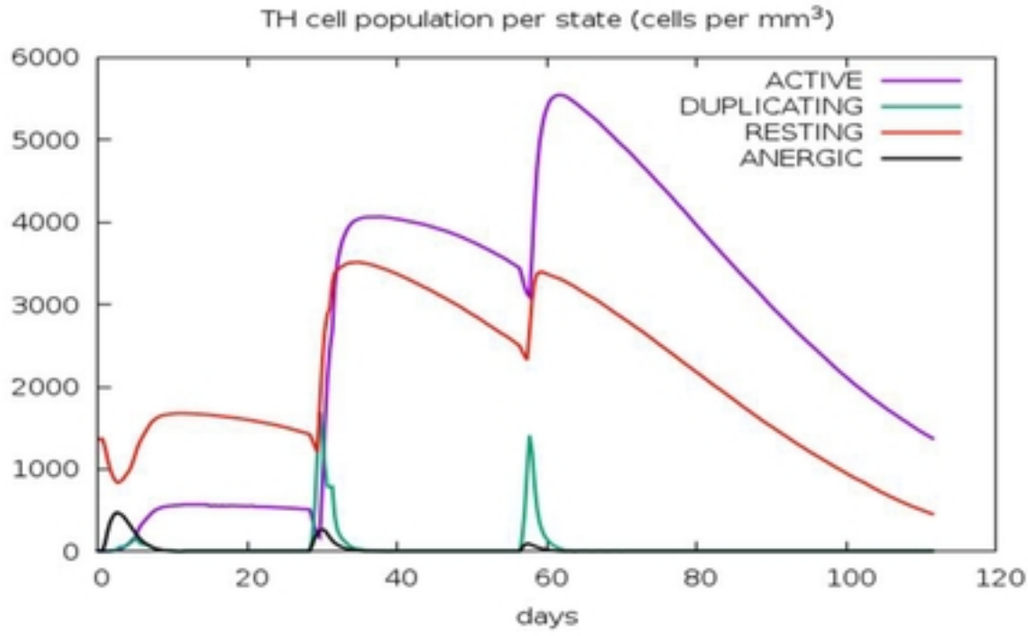
TH cell population per state (cells per mm³)
ACTIVE
DUPLICATING
RESTING
ANERGIC
days

c

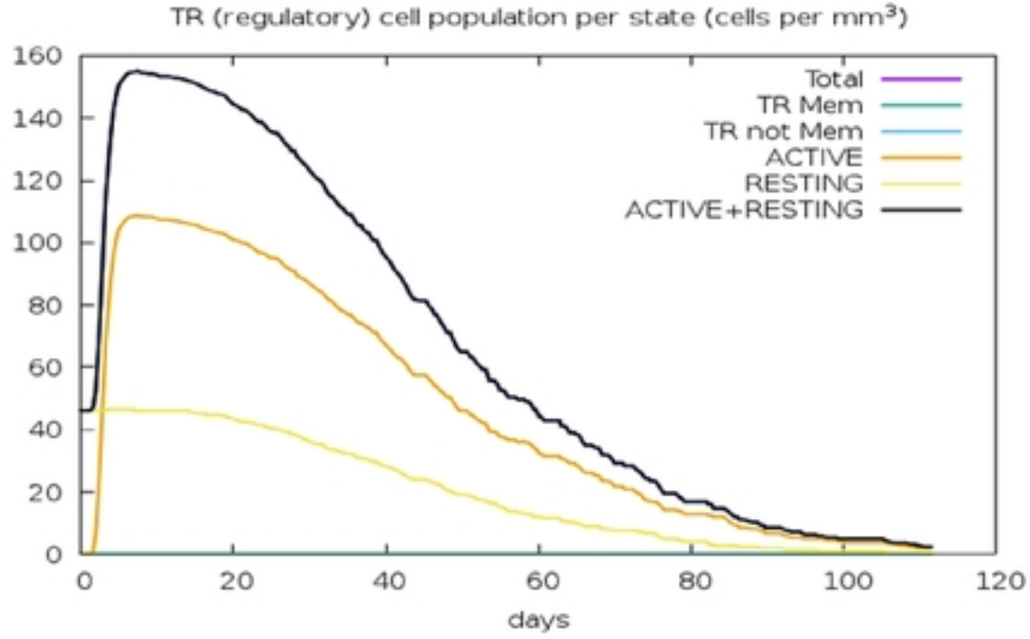
TR (regulatory) cell population per state (cells per mm³)
Total
TR Mem
TR not Mem
ACTIVE
RESTING
ACTIVE+RESTING
days

d

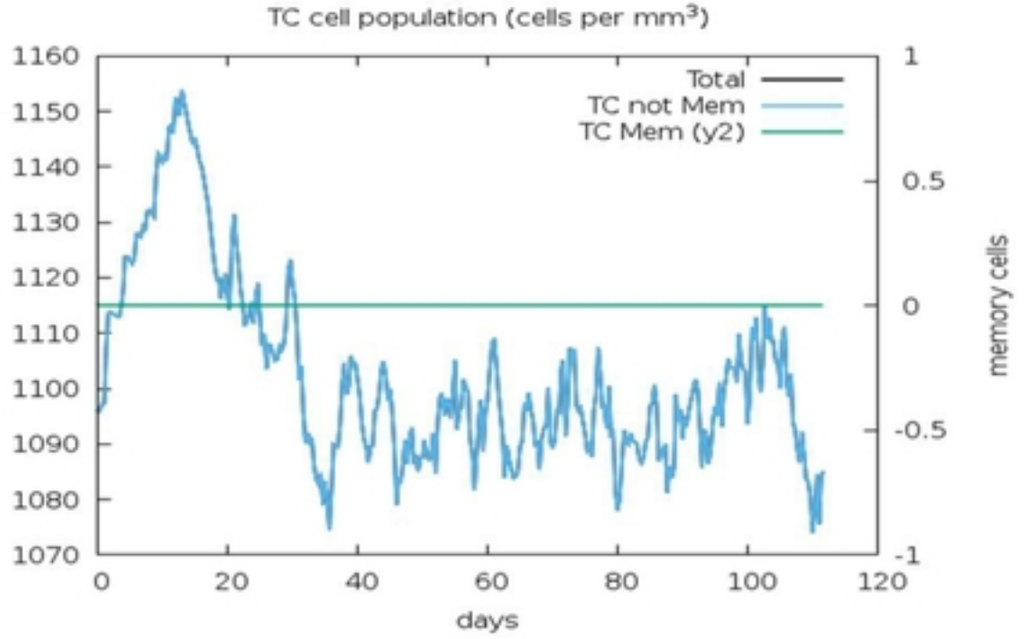
TC cell population (cells per mm³)
Total
TC not Mem
TC Mem (y2)
memory cells
days

Fig 13

a

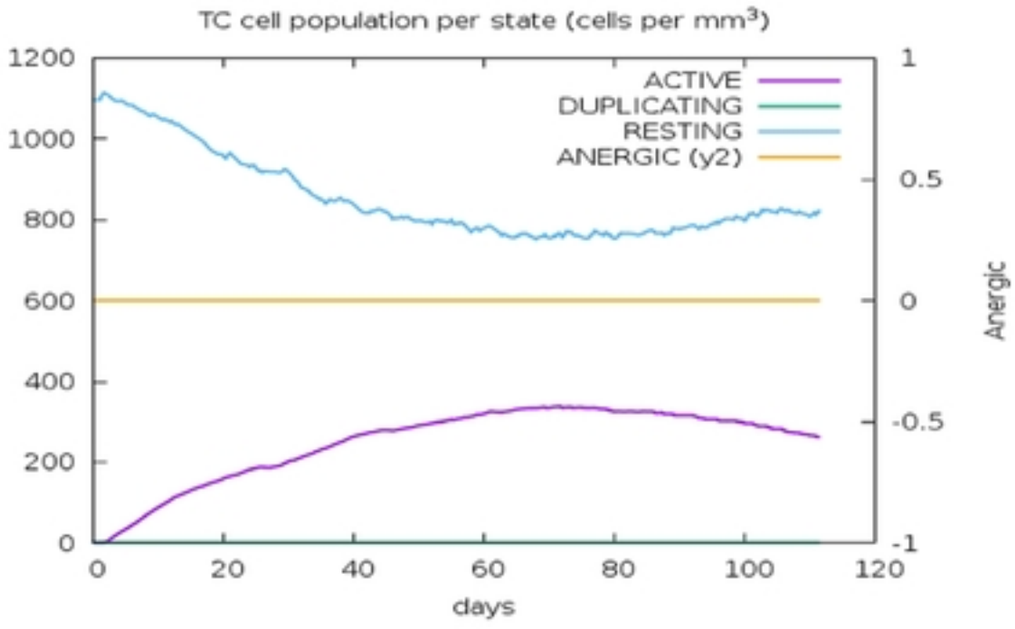
TC cell population per state (cells per mm³)
ACTIVE
DUPLICATING
RESTING
ANERGIC (y2)
Anergic
days

b

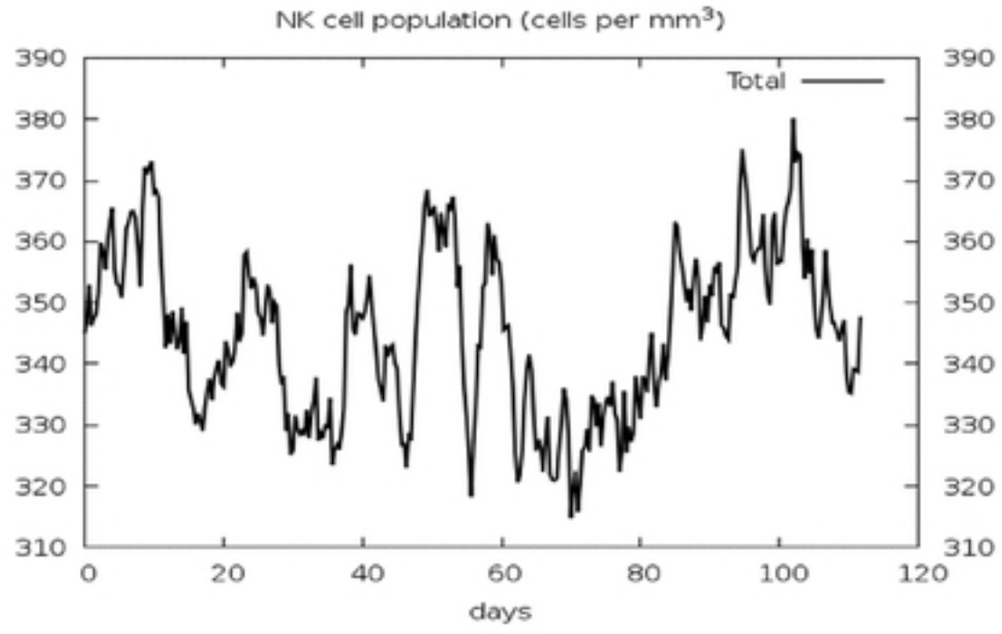
NK cell population (cells per mm³)
Total
days

c

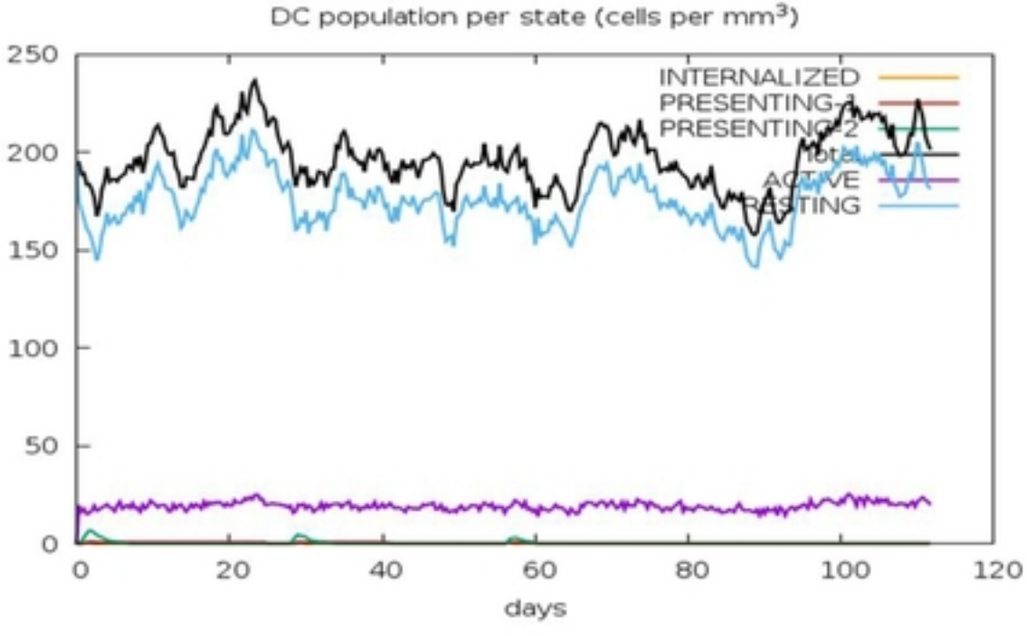
DC population per state (cells per mm³)
INTERNALIZED
PRESENTING-1
PRESENTING-2
Total
ACTIVE
RESTING
days

d

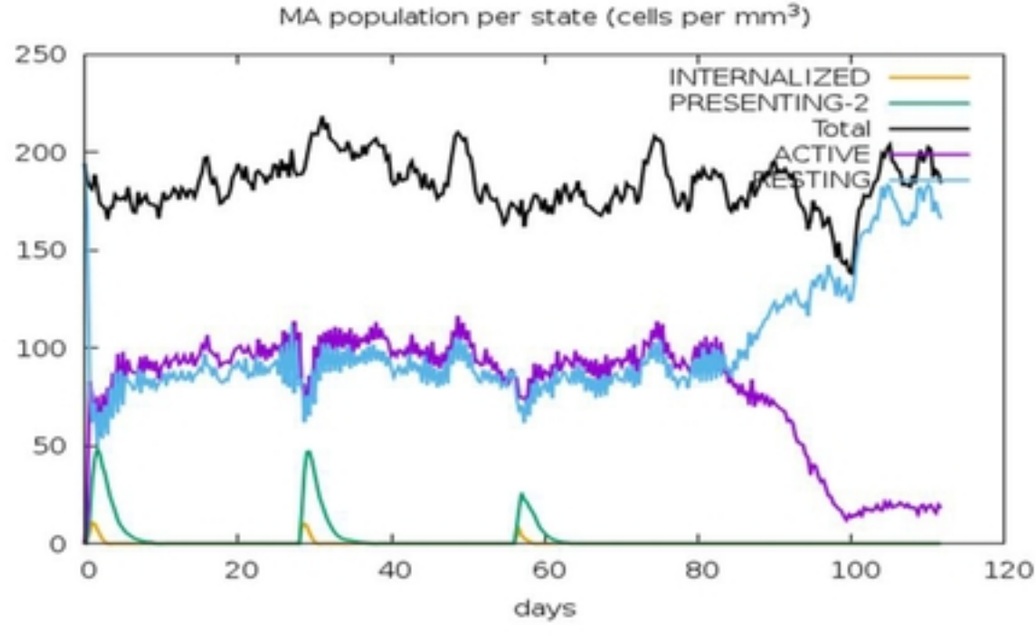
MA population per state (cells per mm³)
INTERNALIZED
PRESENTING-2
Total
ACTIVE
RESTING
days

Fig 14

a

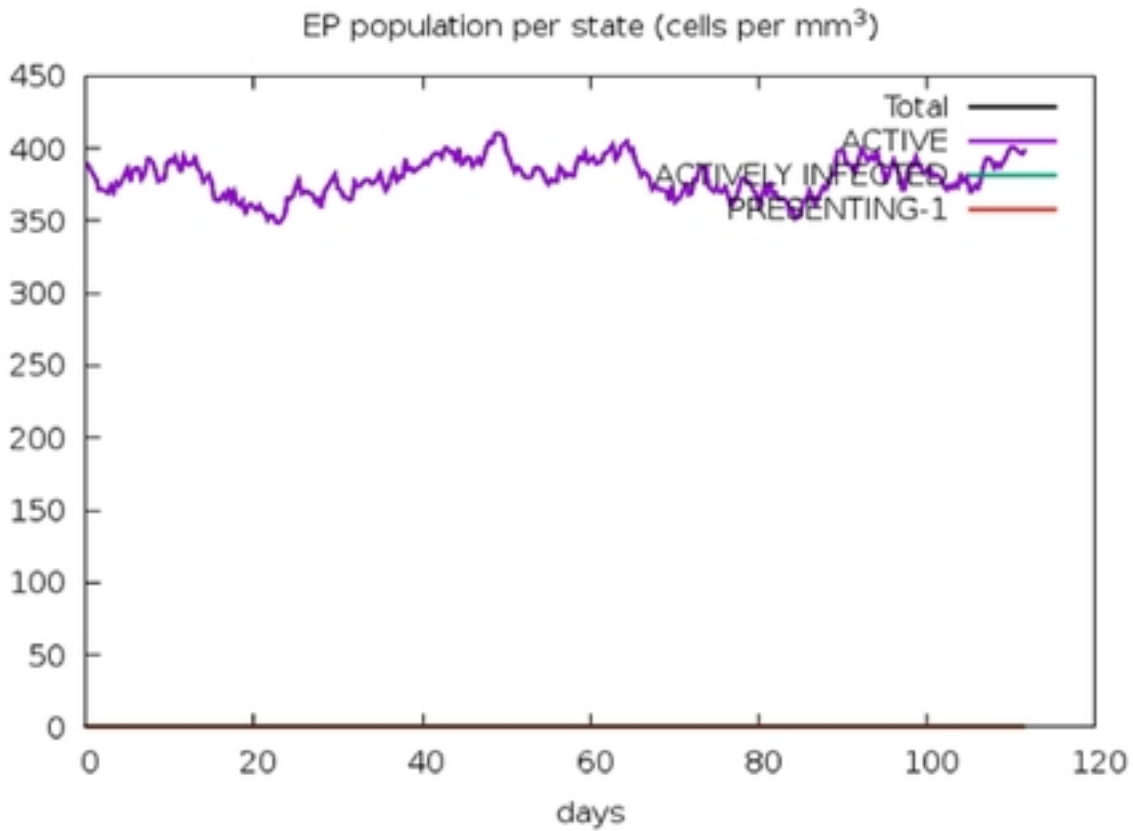
EP population per state (cells per mm³)
Total
ACTIVE
ACTIVELY INFECTED
PRESENTING-1
450
400
350
300
250
200
150
100
50
0
0
20
40
60
80
100
120
days

b

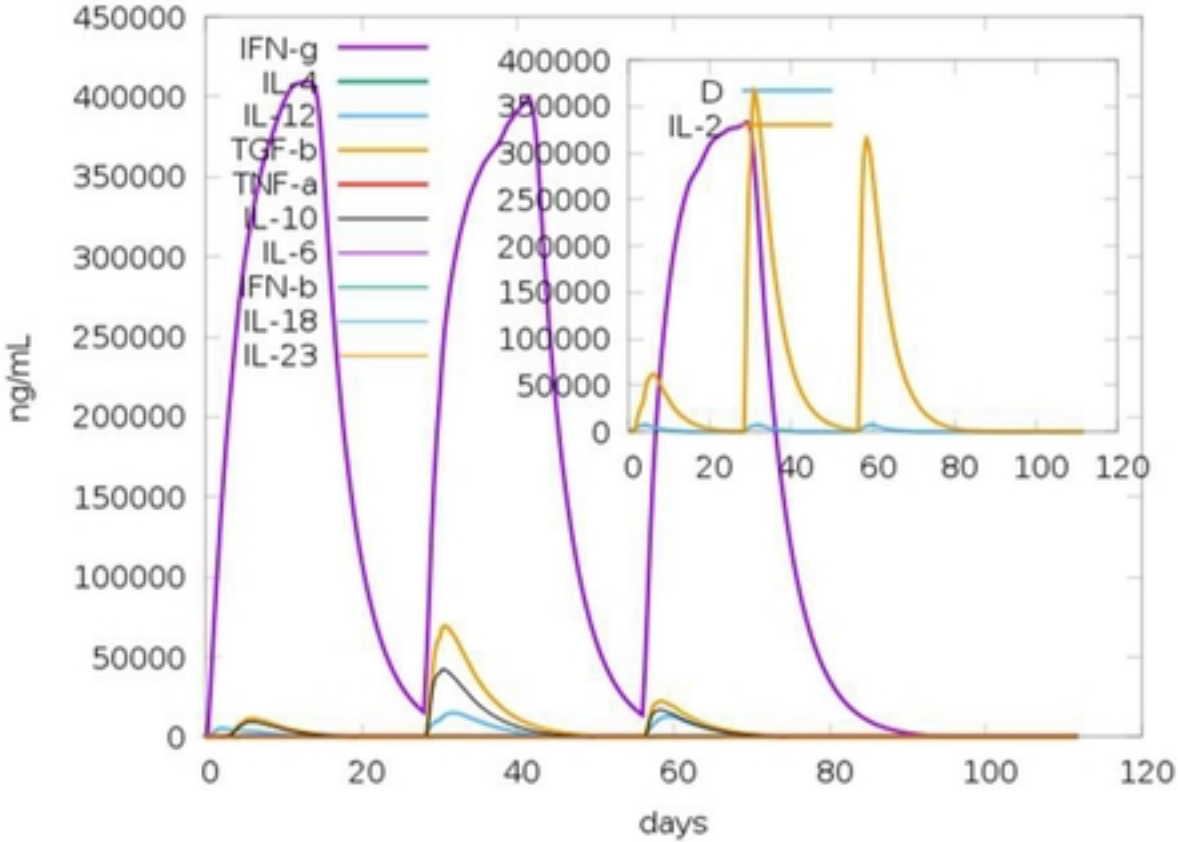
IFN-g
IL-4
IL-12
TGF-b
TNF-a
IL-10
IL-6
IFN-b
IL-18
IL-23
D
IL-2
ng/mL
450000
400000
350000
300000
250000
200000
150000
100000
50000
0
0
20
40
60
80
100
120
days

Fig 15

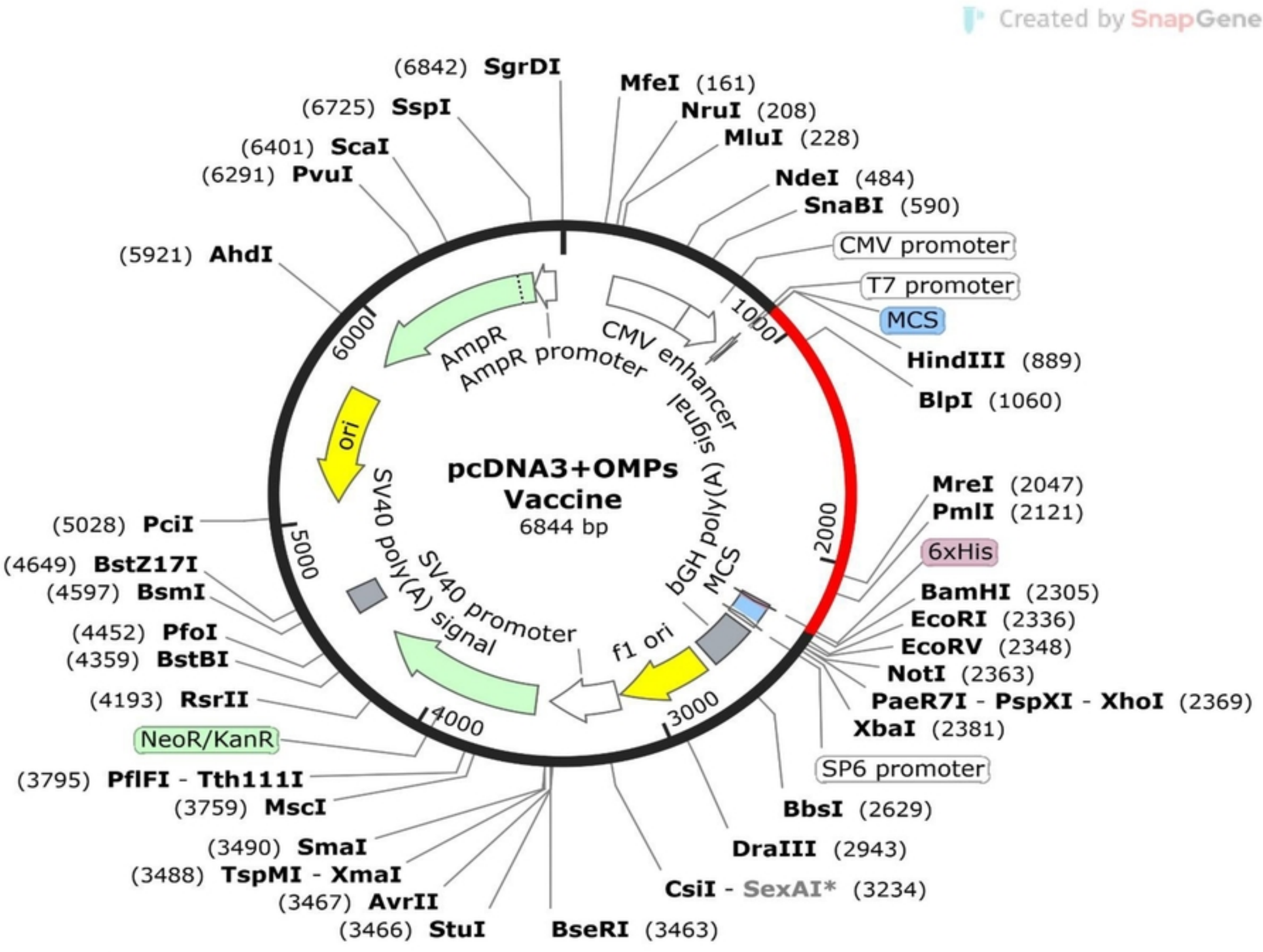
Created by SnapGene
pcDNA3+OMPs
Vaccine
6844 bp
(6842) SgrDI
(6725) SspI
(6401) ScaI
(6291) PvuI
(5921) AhdI
(5028) PciI
(4649) BstZ17I
(4597) BsmI
(4452) PfoI
(4359) BstBI
(4193) RsrII
NeoR/KanR
(3795) PflFI - Tth111I
(3759) MscI
(3490) SmaI
(3488) TspMI - XmaI
(3467) AvrII
(3466) StuI
BseRI (3463)
CsiI - SexAI* (3234)
DraIII (2943)
BbsI (2629)
SP6 promoter
XbaI (2381)
PaeR7I - PspXI - XhoI (2369)
NotI (2363)
EcoRV (2348)
EcoRI (2336)
BamHI (2305)
6xHis
PmlI (2121)
MreI (2047)
BlpI (1060)
HindIII (889)
MCS
T7 promoter
CMV promoter
SnaBI (590)
NdeI (484)
MluI (228)
NruI (208)
MfeI (161)
1000
2000
3000
4000
5000
6000
AmpR
AmpR promoter
CMV enhancer
bGH poly(A) signal
MCS
f1 ori
SV40 promoter
SV40 poly(A) signal
ori

Fig 16